Towards a steerable multi-module soft robotic endoscope for NOTES applications

J.A. (Jan) Lenssen

MSc Report

Committee:
Dr.ir. H. Naghibi Beidokhti
Dr.ir. M. Abayazid
Dr.ir. P.C. Breedveld
Dr.ir. J. Hazrati Marangalou

June 2019

020RAM2019
Robotics and Mechatronics
EE-Math-CS
University of Twente
P.O. Box 217
7500 AE Enschede
The Netherlands

Summary

The current trend in surgery is moving from open surgery to Minimally Invasive Surgery (MIS) and Natural Orifice Transluminal Endoscopic Surgery (NOTES) and patient trauma and recovery times are decreasing. A tool that is used extensively in MIS and NOTES is the endoscope of which rigid and flexible types are available. Rigid endoscopes are good for interaction close to the point of entry, but have difficulty reaching targets that lie behind other organs, while flexible endoscopes can reach these targets, but do not offer the required precision. This is why many studies are performed on flexible endoscopes that are steerable.

Steerable endoscopes can be realized using soft robotic elements, or modules, that, by being inherently compliant, further increase the safety of the devices. The downside of the compliance of soft robotics is that their design and control are harder compared to their rigid counterparts. At the Robotics and Mechatronics group at the University of Twente a soft robotic endoscope module, MOLLUSC, was designed and tested that is pneumatically actuated, based on the work of STIFF-FLOP. The design is compatible with Magnetic Resonance Imaging and can therefore be used in surgery under guidance of MRI. This opens new possibilities for the precision of surgery. While promising, MOLLUSC, STIFF-FLOP, and other similar endoscopes are not used in clinical practice yet and this is partly because these designs are not scalable. Scalability of the multi-module endoscope is an important factor in the applications of MIS and NOTES.

MOLLUSC was characterized and could be steered, but a multi-module endoscope was not realized. This study therefore aimed to realize the MR-compatible soft robotic endoscope system based on this module. In order to achieve this, an in depth analysis of the actuation of this type of module was performed first. A 3-chamber inner sheath module was found to be optimal for minimization of required hardware and for control due to its repeatable behaviour. This module was chosen as the basis of the multi-module endoscope.

Predictable behaviour of the endoscope is necessary in order to control the configuration of the endoscope during surgery, so that collisions and the resulting trauma can be avoided. This predictablity was therefore assessed with fabricated modules and a physical model from literature was implemented that could predict the behaviour of the modules based on the applied chamber pressures. The model turned out not to be adequate and was therefore extended to better describe the endoscopic modules.

Using hardware and software developed for controlling pressure regulators and solenoid valves, the pressures of the pneumatic chambers of the modules could be set precisely and according to a predetermined pattern. With the implementation of the physical model, the bending angle of the endoscopic modules could be controlled to within an error of at most 4°. Accuracy could be significantly improved by extending the model to include the pressure versus bending characterization of the module.

The control system and the endoscopic modules were combined to realize the soft robotic endoscope system. In validation it was found that external influences significantly changed the response of the endoscope. Scalability of the endoscope was then improved by the addition of pneumatic 'airlocks' that could be used to set the pressure of all chambers independently, but from the same supply line. This minimized the required hardware and influence of supply lines running through the endoscope. It was proven possible to control the 3-module endoscope using a single pressure regulator. The whole actuation range that lay within the pressure limits of the hardware could be reached.

The insights gained in this study can be used for working towards endoscopic modules that are to scale and that can be combined to form an MR-compatible soft robotic endoscope suitable for MIS and NOTES.

Preface

The work in this report has benefited from the collaboration and discussions with other people:

The basis of the text of chapter 3 in this report is a manuscript about the design aspects of the endoscopic modules that I have written in close collaboration with Hamid Naghibi Beidokhti and Momen Abayazid for the IEEE International Conference on Soft Robotics (RoboSoft 2019). It was accepted in January of 2019. All finite element simulations for this submission (and subsequently this report) were performed by Hamid. Hamid and Momen were of course also the people that supervised my graduation project and I have gained a lot from the discussions with both of them.

I have had multiple discussions with Jornt Lageveen on the requirements for the endoscope, the improvements that could be made to the amount of bending of the endoscopic modules, and the methods we could use for measuring and characterizing the behaviour of the fabricated modules. Jornt also provided the links to the sources with information on the application of the endoscope, such as the typical anatomy of the large intestine and the path planning algorithms that would be used.

Yoeko Mak helped me setting up and using the EM tracker for performing measurements for characterization and provided the clues on how to calculate the measured bending angles from the raw data. He also helped me with the camera calibration for the photos taken for chapters 6 and 7.

Sander Smits and Henny Kuipers helped me realize the 3D-printed parts and also provided a lot of practical tips on 3D-printing and working with the Ecoflex materials.

Contents

1 Introduction

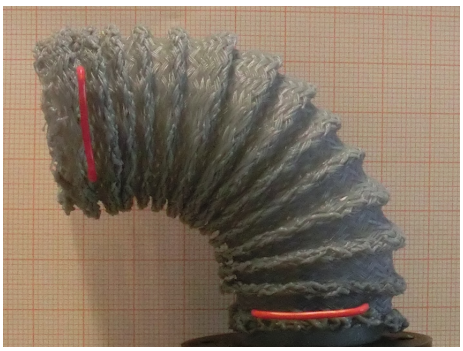

Figure 1.1: MOLLUSC module bending (Jansen, 2018)

1.1 Context of research

The current trend in surgery is moving from open surgery towards Minimally Invasive Surgery (MIS) and Natural Orifice Transluminal Endoscopic Surgery (NOTES). This reduces patient trauma and improves recovery time after surgery. MIS and NOTES procedures require special tools and a tool that is used extensively is the endoscope. With MIS and NOTES having these advantages, different types of endoscopic tools have been created that can not only inspect, but perform surgery as well.

Rigid endoscopes are good for interaction close to the point of entry, but have difficulty reaching targets that lie behind other organs. In endoscopy there is an increasing trend towards the steerable flexible endoscope. Compared to rigid endoscopes, steerable flexible endoscopes give more flexibility to reach difficult targets and make it possible to minimize damage due to contact with the patient. This further decreases trauma as a result (Boškoski and Costamagna, 2018; Seah et al., 2018; Loeve et al., 2010).

Within the set of steerable flexible endoscopes, there are designs that are made completely out of soft materials. The advantage of this type of manipulators is that they can be safely used within applications using Magnetic Resonance Imaging (MRI), giving possibilities for localization using MR. Soft robotic endoscopes are inherently compliant, which means that they are safer than their hard counterparts as well (Rus and Tolley, 2015), (Trivedi et al., 2008). On the other side, compliance of soft robotic modules makes their design and control harder and many studies focused on modelling their behaviour in the last decade (Elsayed et al., 2014; Cianchetti et al., 2014; Sadati et al., 2017).

While many studies have been performed on the design of soft robotics (Laschi et al., 2016), few soft robotic, multi-module endoscope designs were developed and they have not been used in clinical practice. An advanced design is STIFF-FLOP (Gerboni et al., 2015; Allaix et al., 2017), which has already been tested in simulations in an actual surgical environment in a cadaveric setting (Allaix et al., 2017). The endoscope modules within the STIFF-FLOP project contain pneumatic chambers that can be pressurized to achieve actuation, stiffening channels to provide the required stiffness when the endoscope has to apply force or requires more precision, and a central cylinder that can be used to guide surgical instruments towards their target. The design of STIFF-FLOP is similar to that of (Suzumori et al., 1991) and has been implemented as the base of other studies as well (Gifari, 2018; Naghibi et al., 2019; Gerboni et al., 2015; Holdar and Engeberg, 2018). Despite the availability of various prototypes, the issue of scaling is still a problem. Downscaling the manipulator is not straightforward and results in functions being left out (Cianchetti et al., 2014).

Based on the module of STIFF-FLOP, Gifari (Gifari, 2018) designed a new module that solved some of the shortcomings of the STIFF-FLOP design. It enabled multi-level stiffening and provided a higher bending angle when actuating two chambers simultaneously compared to the first design of STIFF-FLOP. At the Robotics and Mechatronics group at the University of Twente (RaM) this module, Multi-LeveL Stiffness Controllable (MOLLUSC), was designed, built and characterized. It can be seen in figure 1.1.

1.2 Shortcomings in the current state-of-the-art

Although MOLLUSC was successful in achieving higher bending angles when two chambers are actuated simultaneously, the endoscopic module did not achieve the expected behaviour at all bending directions. Next to that, while multi-level stiffening was achieved, the behaviour was dependent on the actuation order and externally applied load. The module therefore has not been used in a multi-module configuration and an actual endoscope has not been tested yet.

Later iterations of STIFF-FLOP achieved higher bending angles with two chamber actuation, compared to single chamber actuation, as well. The stiffening capabilities were dropped in order to make space for larger pressure chambers to compensate for the lower bending angle per unit of pressure in this design (Fraś et al., 2015). Although a multi-module configuration was designed and tested, the results and the lack of stiffening capabilities showed that the design was not scalable. A smaller version of STIFF-FLOP (Abidi et al., 2018) was made from two endoscopic modules instead of three. The lack of scalability limits the use of the design in actual surgery, especially in NOTES, as the endoscope must be able to bend around multiple corners and requires a length above 150cm (Whitmer, 2007).

1.3 Research question

This project focusses on the goal of realizing a steerable endoscope from soft materials that is MR-compatible. Starting with an existing endoscopic module design, there are still many aspects of the endoscope that have to be researched.The following research question therefore defines the work of this project:

How can an MR-compatible soft robotic endoscope system be realized for MIS and NOTES applications?

The research question will be answered by trying to achieve the following goals:

- Defining a set of requirements that the multi-module endoscope has to meet.
- Using the most suitable module for the MR-compatible soft robotic endoscope and knowing how to control the individual modules.
- Building a control system that takes position or configuration setpoints and makes the endoscopic modules follow the commands.
- Creating a multi-module endoscope from the chosen module and ensuring that feedforward control of the endoscope is possible (not accouting for disturbances), so that a predetermined path or configuration can be followed.
- Ensuring the scalability of the endoscope in the design, so that further research can focus on decreasing its size and making the endoscope suitable for tests with MIS and NOTES.

1.4 Contributions

The contributions of this work can be summarized as follows:

Insight is gained in the actuation principles of the snake-like soft robotic modules that form the basis of STIFF-FLOP and MOLLUSC and the basis of this work as well. Based on this insight, the most suitable module for the application in terms of scalability and control is chosen and realized. Most research is focussed on the design of the individual modules in terms of achievable bending, while this work focusses on the design aspects that are important for creating a multi-module endoscope based on application requirements. This means that achieving large bending angles is not necessarily required. The scalability of the soft robotic endoscope is improved by the use of micro-pneumatic airlocks that can be used to address the pneumatic chambers in the endoscope. Validations of all design choices gives insight in the principles that govern the behaviour of the endoscope and the design aspects that are important for the multi-module endoscope. While many aspects of the endoscope are left for improvement, the results in this report are the basis for the further optimization of the soft robotic endoscope system that improves MIS and NOTES.

1.5 Approach and report outline

1.5.1 Background knowledge

The required general background knowledge of this work is treated in the chapter 2. This chapter will look at the previous work in the field of soft robotics and focusses on the aspects required for surgical endoscopes. This chapter contains general information and forms the basis for the theory in the core chapters.

1.5.2 Core chapters

The different aspects of the soft robotic endoscope system itself will be covered in dedicated core chapters showing the (theoretical) analysis, design, verification and discussion of the results.

Design aspects of the endoscopic module

One of the most important aspects of the endoscope is the actuator module itself. In order to steer the multi-module endoscope, it should be clear how to control an individual module first. In chapter 3 an in depth analysis of the actuation of the module will be performed using literature, analytical models and simulations. This will be used to pick the best design aspects that form the basis for the module design in the next chapter.

Module fabrication and characterization

The result of the analytical study is the alteration of the existing module so that it becomes better suited for the endoscopic system. The fabrication and characterization of the new module will be treated in chapter 4. The new design is characterized in order to test the theory of the previous chapter. An analytical model of the endoscopic module is made, which can be used to predict the amount of bending and the bending direction dependent on the applied chamber pressures. The characterization of the module will be used for finetuning this model and in the design of the subsystems and software required for controlling the endoscope.

Steering the endoscopic modules

Hardware and software are required in order to be able to control the endoscopic module. The endoscopic system sets certain requirements for the implementation. In chapter 5 the basic system design of the endoscope will be treated, with a focus on the hardware and software that was realized. It will be made clear how the endoscopic module can reach a desired target.

The steerable multi-module endoscope

The fabrication process and verification of the actual multi-module endoscope is the focus of chapter 6. With the basic endoscope completed, the control software has to be altered in order to steer the multi-module implementation. The kinematics of the endoscope will be treated and a test setup is built in order to verify the behaviour of the endoscope.

Scalability

With poor scalability being one of the largest issues with the pneumatic soft robotic endoscope, a novel method of actuating the endoscope with micro pneumatic valves, or airlocks, is explored in chapter 7. This method could significantly reduce the required pneumatic hardware and especially the necessary tubing. The airlocks are designed and fabricated, and their behaviour is characterized. The final airlock design is added to the multi-module endoscope and the working principle is verified using the test setup together with dedicated software.

1.5.3 Discussion, recommendations and conclusion

In chapter 8 this report is conluded with a general discussion on the soft robotic endoscope system and sections dedicated to the recommendations for further research. A conclusion that answers the research question is given in chapter 9.

2 Robotic endoscopes and soft robotics in literature

2.1 Robotic endoscopes for MIS and NOTES applications

2.1.1 MIS and NOTES

Minimally Invasive Surgery (MIS) and Natural Orifice Transluminal Endoscopic Surgery (NOTES) are surgery techniques in which trauma to the patient is minimized by either using small incisions and dedicated small tools (MIS), or using no incisions at all (NOTES). Minimizing trauma helps reducing the negative impact of surgery and thereby improves recovery time.

MIS is performed by making small incisions in the body close to the area of interest. An example of MIS can be seen in figure 2.1. Usually, trocars are placed that help guide the surgical tools towards their target. Because of the limited space available during surgery, visibility is acquired using endoscopes, which are small cameras that can enter the body. These endocopes are usually stiff so that precise manual positioning is possible. The disadvantages of this stiffness is that it is very hard to reach behind organs, making surgery that is not close to the point of entry very difficult.

NOTES is surgery that is performed via the natural holes of the body, so that no incisions are required. Because of this, the tools required have to follow the natural path within the body and therefore have to be flexible. This flexibility assists in reaching the surgical target, but can also lead to positioning difficulties and painful collisions.

MIS and NOTES therefore put resctrictions on the tools that can be used. The other way around, there exist tools that enable MIS and NOTES by introducing new ways of reaching or interacting with target organs. A steerable endoscope that can be used for surgical intervention is a tool that enables MIS and NOTES by making it possible to reach targets that lie behind other organs and to avoid obstacles.

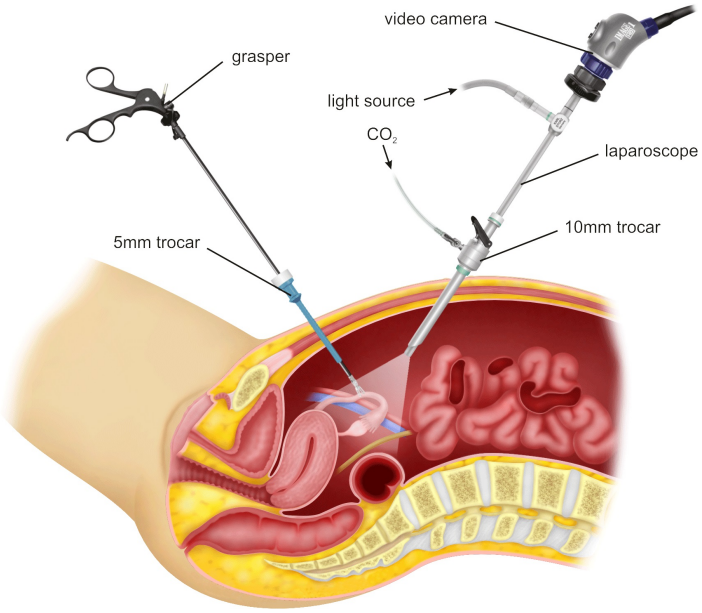

Figure 2.1: An example of Minimally Invasive Surgery with the use of an endoscope (Laparoscope, 2019)

2.1.2 Robotic endoscopes in literature

Several robotic endoscopes exist that can not only inspect, but perform surgery as well. Gifari (Gifari, 2018) performed a literature study listing the different designs and their advantages and disadvantages in the context of MIS and NOTES. The review looks at state-of-the-art robotic endoscopes and lists Invendoscopy (Rösch et al., 2008), Neoguide (Peters et al., 2018), MINIR (Kim et al., 2017), Meshworm (Bernth et al., 2017) and STIFF-FLOP (Cianchetti et al., 2014). While Neoguide meets all requirements set, the final requirement added later, for MR-compatibility, is not met. Having a robotic endoscope that is MR-compatible introduces many options for localization of the endoscope that can assist in surgery.

An MR-compatible endoscope does not include metals and can not use electronic signals within the endoscope itself. Doing so would lead to dangerous situations with the high magnetic field of the scanner or would result in distortions in the images. By making the endoscope MR-compatible, the images of the MRI can be used to steer the robotic endoscope towards its target. A mix of different sensor techniques is then available to correct for any disturbances. The research in the use of MRI during surgery is also closely related to other research performed at RaM, such as the MURAB project (RaM, 2019b) and MRI-compatible robotics (RaM, 2019a).

2.1.3 STIFF-FLOP and MOLLUSC

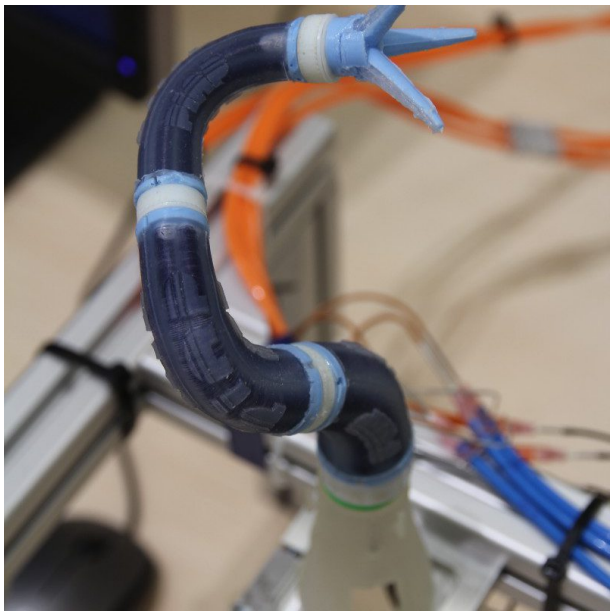

Figure 2.2: STIFF-FLOP (PIAP, 2019)

An advanced soft robotic endoscope design is the Stiffness Controllable Flexible & Learnable Manipulator for Surgical Operations, or STIFF-FLOP (Cianchetti et al., 2014; Abidi et al., 2018), seen in figure 2.2. This design is potentially MR-compatible as it works by pneumatic actuation and contains no materials that can interfere with the MRI. The modules of STIFF-FLOP contain three pneumatic chambers that elongate and bend the module when air pressure is applied, as can be seen in figure 2.3. Different methods of sheathing (in the different versions of the module) constrain the radial expansion of the manipulator and make sure the air pressure is used for the actuation only. Although it is advanced, the design of STIFF-FLOP has not been used in clinical practice. The reason for this is that the design could still be improved a lot before it is actually suitable for surgery.

One of the problems of the first version of STIFF-FLOP was that its bending behaviour was dependent on the actuation order of the chambers and that activating two chambers simulta-

neously would decrease the maximum bending angle of the module. Activating two chambers simultaneously is necessary for using all degrees of freedom (DOF) of the manipulator. Although this problem was fixed in a later STIFF-FLOP design, this new design lacked the stiffening mechanisms required for precision and force during surgery. For this reason Gifari designed a new module based on the first version of STIFF-FLOP containing four pneumatic chambers and granular jamming sacs, integrated in the pneumatic chambers, for stiffening (Gifari, 2018).

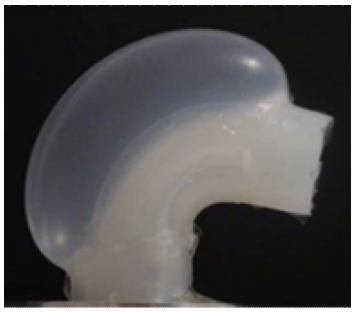

Figure 2.3: A STIFF-FLOP module bending due to applied air pressure (without sheathing that constrains radial expansion) (Cianchetti et al., 2013)

The design of the endoscopic module of Gifari is the starting point of this research towards a multi-module endoscope based on pneumatic actuation.

2.2 Soft continuum actuators

2.2.1 Soft robotics

There is an increasing trend in the use of soft materials in surgical and non-surgical applications. The biggest advantages of using soft materials is that they are safer for interaction, that they enable new actuation methods, and, relevant for this research, that they can be MR-compatible (Rus and Tolley, 2015; Laschi et al., 2016). The downside of soft robots is that they are inherently compliant. While this makes them safer to use, it also means that disturbances have a significant influence on the behaviour of the actuators. This means that the design and control of soft robotics is harder and that modelling is not trivial. Some examples of soft robotics are a soft robotic gripper based on particle jamming (Brown et al., 2010), which shows a new form of actuation, a soft robotic glove for rehabilitation (Polygerinos et al., 2015), which is safer than the alternatives, and of course the MR-compatible soft robotic endoscopes STIFF-FLOP and MOLLUSC.

As modelling of soft robotics is harder than modelling rigid link robotics, methods have been developed that aid in approximating the kinematics of soft robotics by rigid link kinematics, so that conventional and successful techniques can still be used.

2.2.2 Kinematics

The soft robotic endoscope can be seen as a multisegment robot arm. Each segment can be actuated and the end effector position will be determined by the kinematics of the whole. The difference between the soft robotic endoscope and a standard robot arm is that the endoscope has no rigid links, which means that the kinematics are not straightforward. This is a known problem in soft robotics and several control strategies have been designed to overcome this problem (Webster III and Jones, 2010).

Instead of having links and joints, the segments of the soft robotic endoscope bend over the whole length. Jones and Walker (Jones and Walker, 2006) show that this bending can be approximated using a curve with constant curvature. In this way, if the curvature, direction and

elongation of all modules are known, the position of the end effector can be determined as well. This means that three parameters per segment are required for describing the configuration of the robot. A schematic representation of the constant curvature approximation and the three associated parameters is given in figure 2.4.

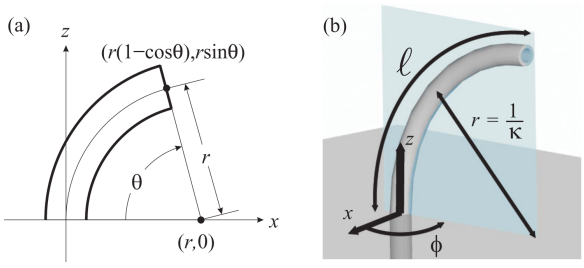

Figure 2.4: The constant curvature approximation showing how three parameters are required to fully define the shape of a bending soft robotic snake-like module. (a) is a side view showing how the bending angle θ and the curvature radius can be used to find the location of the tip of the module. (b) is a 3D view showing that the radius is directly related to the curvature κ of the module and that the bending direction is defined by ϕ. While the bending direction ϕ is independent of the other variables, κ, l and θ are all linked. Only two of these three variables are necessary for completely defining the bending shape. In constant curvature kinematics κ, l and ϕ are used. r and θ can be calculated when desired. (Webster III and Jones, 2010)

Jones and Walker (Jones and Walker, 2006) give a method for mapping these three parameters to the standard rigid link kinematics. In this way, the problem of controlling the soft robot can be limited to the hardware. Standard techniques can be used until the pressures for the pneumatic chambers have to be determined using a specific mapping. The characterization of the bending angle dependent on chamber pressures of the endoscope has to be used then. Figure 2.5 shows the different spaces for describing the kinematics and the mappings between them.

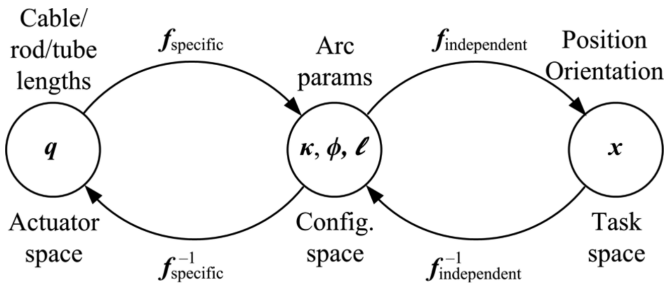

Figure 2.5: Mapping between different spaces in constant curvature kinematics (Webster III and Jones, 2010). The actuator space is defined by the behaviour of the actuators and is therefore specific for a certain actuator design. The configuration space is defined by the constant curvature approximation of the robot and contains the values of the three paramters (κ, ϕ, and l) per module. The task space is independent of the robot that is used and contains the standard kinematics.

For the pneumatic actuators of the soft robotic endoscope, the specific mapping determines the pressures required for actuation, or the curvature parameters of the robot based on the measured position. The mapping from configuration to actuation has to take external forces into account when the controller has to work in an actual non-ideal environment. This means that effort is required to implement the control of the soft robotic endoscope. Visual feedback can be used to correct the errors from unknown external forces and non-linearities in the de-

sign, but requires extra hardware, in the form of imaging devices such as cameras, and extra software to process the visual information and generate the correct references.

3 Design aspects of the endoscopic module

From literature and experiments it followed that the pneumatically actuated bending cylindrical module, such as STIFF-FLOP and MOLLUSC, is a very suitable candidate for the steerable robotic endoscope application when MR-compatibility is taken into account as well. The designs of STIFF-FLOP, and the improvements of Gifari, therefore form the basis of the soft robotic endoscope. The goal of this chapter is to select a final design that best fits the requirements determined by the system level design requirements, based on this type of module. In order to do this, the working principle of the module will be analyzed first.

This chapter begins with the system requirements of the endoscope so that the requirements of the module can be formulated. These requirements will be checked for different types of cylindrical modules by analyzing the working principle behind the actuation of the modules. A study is performed on the influence of sheathing, the number of pneumatic chambers, and the volumetric design of the pneumatic chambers. Finite element simulations and an analytical model will be used for the comparison between the bending angles of the modules based on the amount of pressure applied. While there are advantages and disadvantages to all design aspects, it is clear that a 3-chamber inner sheath module is the best choice for the soft robotic multi-module endoscope in this application where controllability and scalability are critical.

3.1 Requirements

In order to define the requirements of the endoscopic modules, the requirements for the endoscope (the system requirements) have to be defined first. By making this distinction between module level and system level requirements, the endoscope system level design is not directly dependent on the module design. It is logical that the module requirements follow from the endoscope requirements, but some system level requirements are not dependent on the type of module that is used.

System level requirements

Dimensions MIS and NOTES put strict size limits on the tools that are used. Standard trocar sizes are between 3mm and 10mm (Blinman, 2010), which mean the endoscope diameter should stay below this value in order to be usable. In general, for the diameter of a robotic endoscope, smaller is better to keep the impact minimal, but a tradeoff can be made when other requirements have to be met. No clear requirements on the dimensions of the endoscope will be formulated for this project. Colonoscopes require a length of at least 150cm in order to be able to reach the end of the large intestine, see figure 3.1. The dimensions of the endoscope will follow from the module dimensions and the required dynamics. Because downscaling soft robotic endoscopes is still an open issue, the general requirement is that size constraints should be kept in mind during the design. Scalability has high priority. In order to make the project feasible, however, the endoscope will not actually be made to scale. It will remain a proof of concept.

Dynamics Eventually it should be possible to have a soft robotic endoscope that can follow the whole trajectory of the large intestine. Work on determining the minimum required number of modules is still being done, but that it should be more than three, the usual number of modules in demonstrator models (such as the first version of STIFF-FLOP (Cianchetti et al., 2014)), is already known. The large intestine contains at least six bends, which requires at least six degrees of freedom if the endoscope has to take the shape of the colon. Because the bends are in different directions, six degrees of freedom are not enough if the endoscope has to be pushed through the intestine. At least six modules with two degrees of freedom each are therefore necessary, although the varying distances be-

tween bends require varying non-bending sections between these modules. The length of the non-bending sections should change depending on the position of the tip of the endoscope. This is why the endoscope has to be made up of a series of modules that can achieve the bending radius of the smallest bend. The number of modules is then the total length divided by the length of a single module. For the proof of concept in this project, at least three modules will have to be put in series. Scalability in terms of the number of modules will be a design guideline. Requirements for the elongation of the modules will not be set.

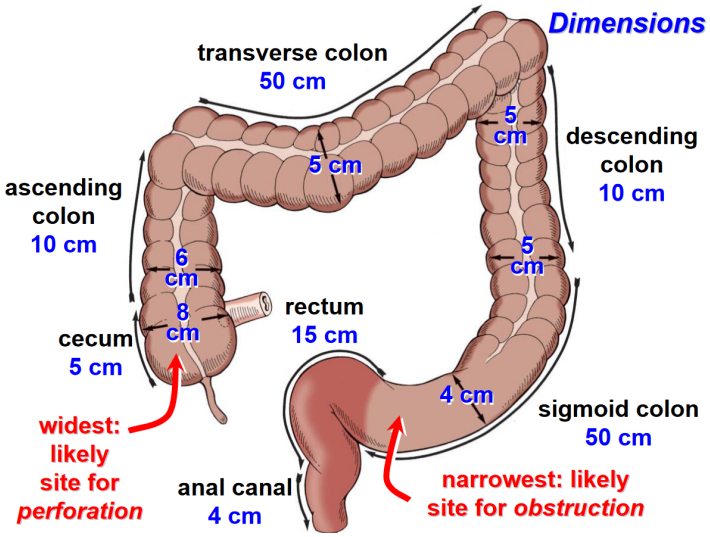

Figure 3.1: Typical dimensions for the large intestine (Whitmer, 2007)

Stiffness The soft robotic endoscope should both be compliant and stiff, depending on the situation. It should be able to support itself, so that contact with the environment can be minimized. This means that the system should have stiffening capabilities for when force or precision is required. Base stiffness should be high (or low) enough so that the dynamic requirements can be met. Stiffness after stiffening is determined by the system design and should be high enough to support the dynamics and control. Because a lot of research has already been performed in the direction of stiffening of soft robotics, and a lot of design options are possible, the endoscope in this project will not contain a stiffening mechanism. A small study was performed on different stiffening mechanisms in literature and the most suitable method seems to be layer jamming (Kim et al., 2012). Layer jamming has the benefit that its design can be viewed separate from the endoscope itself, because the mechanism can be placed outside of the modules. The literature study is not included in this work, but a small summary can be read in appendix A.

Safety Expected safety problems arise around the maximum usable pressure for realizing the bending of the modules and the materials that will be used for the construction. The device should be designed with safety of the patient and operator in mind, but since the endoscope will introduce some new concepts, the safety for the patient will be an aspect left open for improvement. No maximum value for the used pressure will be set.

Control To minimize the risk of trauma the endoscope should follow a determined path during surgery or inspection. This means that the endoscope should support itself and interact with the environment as little as possible. This should be achieved by having a clear mapping between configuration space and actuator space, as defined in the constant curvature approximation. It will be assumed that the path planning will be solved outside of

this study and that feedback on the position and configuration of the whole endoscope is available. Position guarantee in feedforward is therefore not a requirement. Feedforward control, by manual input for example, should be implemented.

Other All parts of the endoscope that have to be close to the patient will be made MRI-compatible. Ferreous materials will be prohibited, as will all other metals, because they pose a large risk towards the safety of the patient and the operator. Electronic signals will not be used close to the patient, as they will interfere as well.

Because this work is based on previous work performed by Gifari and the research focus is on the multi-module endoscope, some requirements for the endoscopic module can already be formulated by looking at MOLLUSC.

Module level requirements

Dimensions With previous work focussing on the design of a single endoscopic module, the dimensions of the individual modules will be adopted from MOLLUSC in the multi-module design. The module will therefore be 45mm in length and have an outer diameter of 25mm, with a central cylinder with a diameter of 8mm in order to guide surgical instruments. These dimensions are not suitable for use in clinical practice and the device remains a proof of concept.

Dynamics Seen from the top, a module should be able to move in all directions in the plane (the bending direction). Pneumatic chambers can only elongate and not contract, which means that only an antagonistic pair of chambers can cause actuation in both directions along a single axis. For actuation in a plane (2D) this means that at least three pneumatic chambers are required. The reason that the minimum is not four is because two chambers spaced at 120° can substitute one of the chambers of the antagonistic pair. This principle is shown in figure 3.2. The minimum required bending angle of the module seen from the side follows from the path planning and is 40° with the specified dimensions of the module. This was determined from simulations by another student at RaM (J.W. Lageveen) and might change with the module dimensions or path planning algorithms in the future.

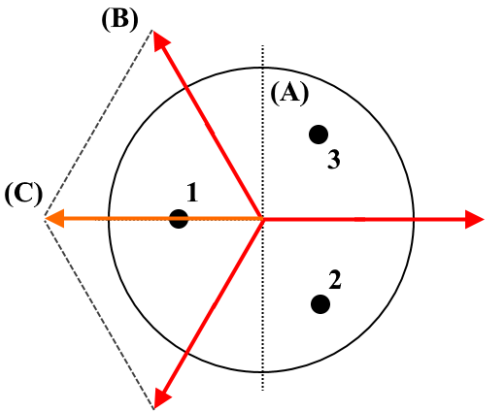

Figure 3.2: Vectors indicating the bending moment during actuation of a 3-chamber module; anatagonistic actuation is possible by three chambers that are spaced 120° apart due to the sum of vectors. The chambers are numbered 1 to 3. (A) is the outside wall of the module, (B) is the moment vector caused by the actuation of a single chamber, and (C) is the net vector when two chambers with the same moment are combined.

While the modules of the type of STIFF-FLOP and MOLLUSC meet the basic requirements, choosing the right design requires insight in the behaviour of the module under actuation. Based on the results of Cianchetti et al, Fraś et al., and Gifari (Cianchetti et al., 2014; Fraś et al., 2015; Gifari, 2018), it is expected that this behaviour differs significantly with each design. So, while a limited set of options is left, the requirements are not clear enough to pick the final design. This is why the bending behaviour of the module will be treated next.

3.2 Study on the theory of bending

The modules bend because pneumatic chambers are pressurized, so that a force is applied that results in elongation and bending of the module. This force is directly proportional to the area of the pneumatic chambers, which means that a higher force is applied when the pneumatic chambers expand radially (bulge as was shown in figure 2.3). This bulging was observed in modules without sheathing and in the modules with outer sheath. The outer sheath of MOLLUSC prevents extreme bulging for example, but the chambers can still expand inwards. This was found by both Fraś et al. (Fraś et al., 2015) and Gifari (Gifari, 2018). In the second and third version of STIFF-FLOP less bending is observed for the same amount of pressure because the chambers do not expand significantly (Fraś et al., 2015).

The number of chambers has a large influence on the bending behaviour of the module as well. One of the improvements of MOLLUSC in comparison to the first version of STIFF-FLOP is based on the number of chambers. This is why a study based on analytical calculations and Finite Element (FE) simulations was performed to gain insight in the design aspects that determine the amount of bending of a module.

Several comparative studies have already been performed on the influence of design choices on the pneumatic chambers of STIFF-FLOP modules and similar soft robotic endoscope modules. Performance of soft actuator modules has been assessed based on the bending angle determined by chamber pressure and volume. Elsayed et al. (Elsayed et al., 2014) compare different pneumatic chamber shapes and their influence on the bending behaviour of the manipulator. Fraś et al. (Fraś et al., 2015) show the differences between two methods of constraining the radial expansion of the endoscope, which reduces the risk of failure of the chambers. The improvement in bending with two pneumatic chambers actuated in a 4-chamber design compared to the 3-chamber design is shown by Gifari and Naghibi et al. (Gifari, 2018; Naghibi et al., 2019). Although informative, these studies each focus on a single issue, even though their design choices cannot be viewed separately.

The impact of the size of the pneumatic chambers was already explained. Dimensional requirements in multi-module endoscope design demand that limited space is shared between pneumatic chambers and components required for fixing multiple modules in series and other functionalities. These components include pneumatic pressure tubes, connector segments, the central cylinder for surgical instruments and stiffening mechanisms. The dimensions of the pneumatic chambers cannot be decreased without increasing the required pressure for actuation. High pressure is not desired, as this poses a risk to patient safety (Cianchetti et al., 2013). A way to overcome this problem is by looking at the volumetric design (lengthwise geometry) of the chambers as well.

The study therefore assesses the influence of the following design aspects of the pneumatic soft module, on the function of the endoscopic module:

1. The methods of constraining radial expansion, or sheathing type
2. The number of chambers
3. The volumetric design

By looking at soft robotic endoscope modules and modelling their behaviour dependent on pneumatic chamber design, this study will provide insights and results that can be used in the system design of a soft, steerable, flexible endoscope, so that the design for the endoscopic module can be finalized.

3.2.1 Evaluation of design aspects of the pneumatic chambers

The analytical static model for position estimation of a soft robotic endoscope module is described by Fraś et al. (Fraś et al., 2014). Using this model, it is possible to predict the general behavior of the modules under various design choices. The amount of elongation of a chamber depends on the stiffness of the module (which is depended on geometry) and the amount of force that is applied in the direction of elongation. The force acting on any cross section of the chamber is proportional to the area and the air pressure (Fraś et al., 2014), which is also why the bulging effect introduces a strong non-linear effect in the pressure versus the bending angle curve. The bulging increases the cross-sectional area of the chamber. This also explains why higher pressures are necessary once the radial expansion of the chambers is constrained. The cross-sectional area of the chamber does not increase, so the bending moment does not increase. Both the non-linear effect due to bulging and the higher required pressure due to radial constraints are demonstrated by Fraś et al. (Fraś et al., 2015).

1) Radial expansion constraint (sheathing) Bulging in the soft pneumatic actuator increases the module diameter and is undesired (Cianchetti et al., 2013). Different methods are being used to constrain the radial expansion of the pneumatic chambers. The designs from Gifari and De Falco et al. (Gifari, 2018; De Falco et al., 2017) use a crimped sheath that surrounds the whole module, keeping its diameter within bounds. While effective in preventing extreme bulging outside of the module, the sheath's irregularities combined with the soft material of the manipulator introduce non-linearities that affect the module's performance, especially when actuating two chambers simultaneously, as is shown by Cianchetti et al. and De Falco et al. (Cianchetti et al., 2014; De Falco et al., 2017). With only the outer sheath limiting the radial expansion of the 3-chamber module, the bending angle with two chambers actuated simultaneously is shown to be much less than the bending angle of the module when only a single chamber is actuated. This is caused by chamber deformation when pressure is applied, leading to a shift of geometrical centers (Fraś et al., 2015). The deformation introduces a dependency on the actuation order as well (Fraś et al., 2015; Gifari, 2018). Two solutions have been proposed to counteract this effect, namely moving the sheath to the inside of the chambers and changing the number of pneumatic chambers.

2) Number of pneumatic chambers Gifari and Naghibi et al. (Gifari, 2018; Naghibi et al., 2019) propose a 4-chamber solution, which can achieve a larger bending angle by actuating two chambers, despite the limitations of the outer sheath. As was explained, only three pneumatic chambers are necessary to reach all angles required by the pneumatic actuator and increasing the number to four does not add any more degrees of freedom, since the fourth chamber's direction of elongation stays parallel to the other three (Jones and Walker, 2006). Nevertheless, using four chambers instead of three chambers is a valid option to increase the possible bending angle without increasing the fabrication complexity. This is because using the 4-chamber design, actuating two chambers simultaneously will result in a larger moment than when a single chamber is actuated (Gifari, 2018; Naghibi et al., 2019). This effect can be seen in figure 3.3 and counteracts the decreasing moment due to the shift in geometrical centers, although the dependency on actuation order remains and more pneumatic hardware is required to be able to control the bending angle.

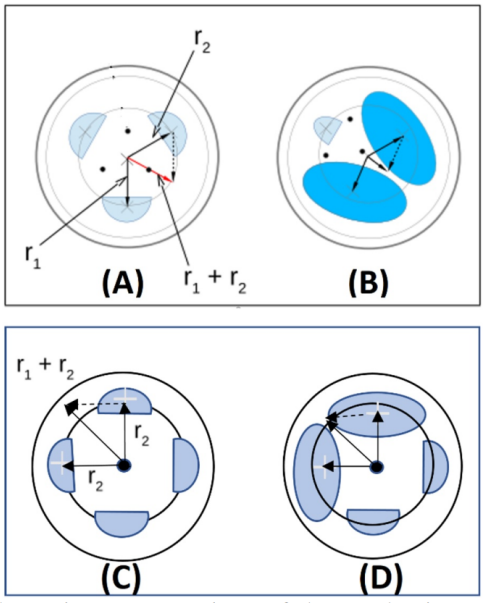

Figure 3.3: Outer sheath modules show shifting of the centers of the actuation chambers when the chambers increase in diameter at higher pressures, this decreases the resulting moment arm when two chambers are actuated simultaneously (Gifari, 2018).

3) Volumetric design of the pneumatic chambers With the knowledge that the area of the cross section of a chamber determines the force with which the stiffness of the chamber walls is overcome, it might be beneficial to look further than just the shape of the cross section of the chambers. This cross section does not necessarily have to be constant over the length of the chamber. While studies have been performed on different shapes of the cross section of the chambers and many different designs of the manipulator were created (Gifari, 2018; Gerboni et al., 2015; Suzumori et al., 1991; Holdar and Engeberg, 2018; Cianchetti et al., 2013), all these studies assumed an equal shape all the way through the length of the chamber. This study will also look into the effects of varying the size or shape of the chamber over the length of the chamber. By being able to shape the whole chamber, instead of only the cross sectional area, there is more freedom to change the space available for other functionalities.

Chamber designs varying their cross section benefit from the method of constraining the radial expansion of the pneumatic chambers, because without this constraint, the chambers would expand into the area that is necessary for other functionalities. With the radial expansion constrained, the volume of the pneumatic chambers can be shaped around the space required for including other functions, such as stiffening methods, as applied in STIFF-FLOP, or routing the pressure tubes or connecting the modules in series, without having to lower the volume of the chamber too much. Although a lower chamber volume decreases the time it takes for a certain pressure to build up, which increases the possible control bandwidth, the volume of the chamber cannot be changed without affecting the pressure required for bending. This is because the bending angle of the whole module is the result of integrating the bending angle of every infinitesimal slice of the module (Fraś et al., 2014).

Taking a circular chamber with constant cross section and then decreasing this cross section in the middle (as in an hourglass, as in figure 3.4 (B)), will result in smaller forces and moments on the part of the module where the cross section has been decreased. This means that the resulting angle will be smaller after integration.

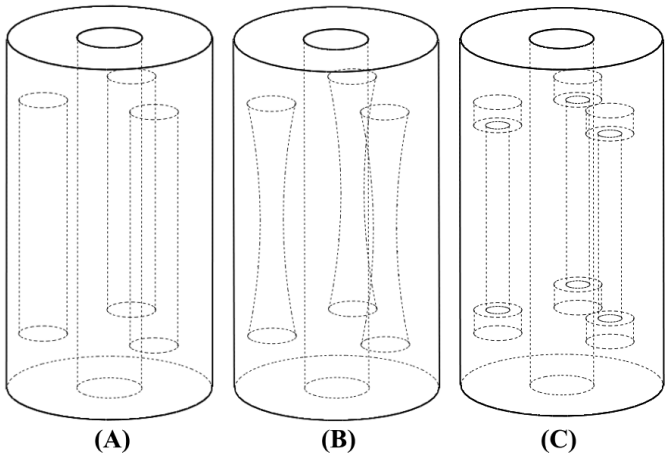

Figure 3.4: The three 3-chamber soft robotic endoscope modules (including empty central cylinder) with different volumetric chamber designs: (A) The basic cylinder design, (B) The concave design, and (C) The sharp edged design.

In theory and regarding the multi-module design and fabrication, the available methods all have their advantages and disadvantages. As a result, comparing different modules using finite element simulations can give a better understanding on the implications of different choices, as described before, on the improvement of the module functionality. The methods for comparing the design aspects will be described next.

3.3 Methods for analyzing the design aspects

3.3.1 Finite Element simulations

A generic finite element model of a soft endoscopic module (figure 3.5) was developed in Abaqus v2018 (Simulia, Providence, RI, USA). A dynamic implicit solver was used with quasi-static simulation. The module was meshed with second-order tetrahedral elements (C3D10) with an average element size of 2mm. Similar to the physical model utilized for validation, the module had a diameter of 25mm and a length of 45mm, with a central cylinder of 8mm in diameter. The total length of the chambers was 30mm, and in all cases, the chambers were configured circumferentially symmetrical around the central cylinder at a radius of 8.25mm.

Different geometrical design aspects were modelled to assess the variations in number of chambers (three versus four chambers) and chamber volumetric profiles. Moreover, in order to evaluate different types of radial expansion constraints or sheathing types, fiberic sheath was applied around either the module body, chamber, or both, using the Holzapfel-Gesser-Ogden hyper-elastic material model. In each case, a linearly ramped pressure from 0 bar to 1 bar was applied to the chambers. The bending of the module tip was extracted at increments of 0.05 bar of input pressure. Finite element simulations have been set up by, and were performed by, H. Naghibi.

3.3.2 Validation of the finite element simulations

First, the finite elements of a 3-chamber and a 4-chamber module with half-circular cross-sectional profile, for which experimental data was available for validation purposes, will be modelled. Outer sheathing around the module body is modelled, and the modules are actuated by applying the pressure to one and two chambers. A total of six different cases are simulated and the bending angle versus pressure curves will be compared to the ones from experiment as follows:

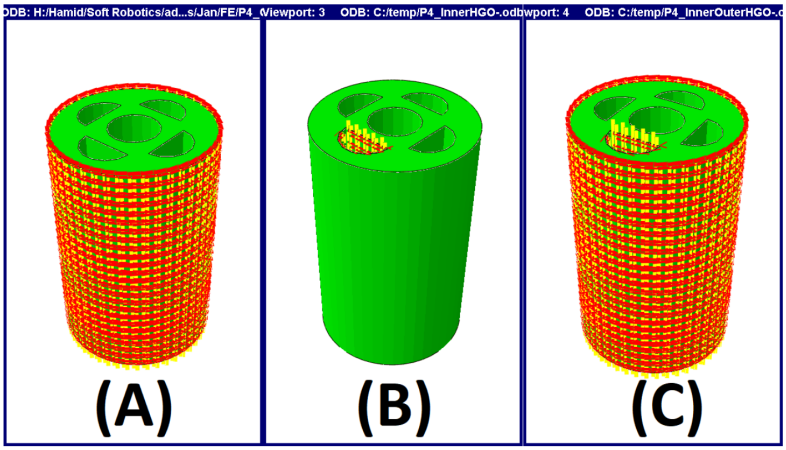

Figure 3.5: The finite element model (cut view) of the 4-chamber module with three different sheathings modelled here as: body (outer) sheath (A), chamber (inner) sheath (B), and both outer and inner sheath (C).

- The simulation of the 4-chamber design with outer sheath for one and two chamber actuations will be compared to the results of the study of Gifari and Naghibi et al. (Gifari, 2018; Naghibi et al., 2019).
- The simulation of the 3-chamber design with outer sheath for one and two chamber actuations will be compared to the results of the old STIFF-FLOP design (Fraś et al., 2015).
- The simulation of the 3-chamber design with inner sheath for one and two chamber actuations will be compared to the results of the new STIFF-FLOP design (Fraś et al., 2015).

3.3.3 Comparing design aspects

1) Radial expansion constraints (sheathing) To investigate the influence of different types of sheathings to constrain the radial expansion, the 4-chamber module was modelled with no sheath, with a sheath around the chamber (inner sheath), with a sheath around the body (outer sheath), and with a sheath around both the chamber and the body (both sheaths).

2) Number of chambers In order to compare the effect of the number of pneumatic chambers, a comparison was made between the 3-chamber and 4-chamber designs with either the inner sheath, or the outer sheath only. In any of the assessed cases, one chamber activation and two chambers activation were simulated. The cross sectional profile was selected to be a half circle with a radius of 4mm.

3) Volumetric design of pneumatic chambers The influence of the volumetric chamber design was investigated by comparing three different designs of the 3-chamber module. As illustrated in figure 3.4, the basic cylinder design (A), an hourglass-shaped concave design (B), and an I-shaped sharp-edged design (C), were modelled and simulated. The chamber cross-sectional profiles were circular in all cases, with a diameter of 6mm which was reduced to 3mm in the concave and extreme sharped edged cases. This was combined with an inner sheath to ensure that this cross section would deform minimally.

3.4 Results

1) Validation of the finite element simulations The results of the simulations and the experiments of Gifari (Gifari, 2018) for the 4-chamber design are shown in figure 3.6a. While

the general trend of the curves is similar, the simulated bending angles of the modules require 0.1 bar less pressure. This offset is mainly expected to be due to a gap between the outer surface of the module and the sheath. The simulation results, therefore, were shifted by 0.1 bar as shown in figure 3.6a. The results of the simulations for the 3-chamber design are shown in figure 3.6b. Experimental results of the 3-chamber STIFF-FLOP module were found by Fraś et al. (Fraś et al., 2015). Despite the slight differences in bending values, the overall trend is similar. The differences in bending can be due to the use of a different chamber cross sectional profile by Fraś et al. This was circular, whereas a half-circular profile was modelled in the finite element simulations.

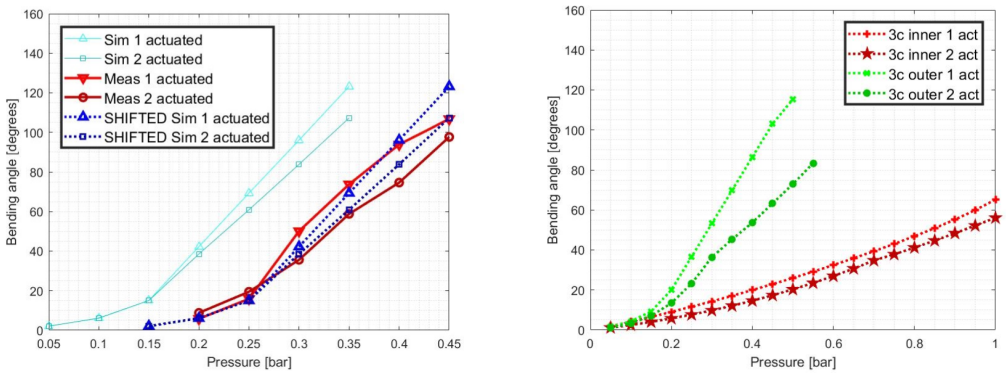

(a) The simulated and experimentally measured performance of one and two chamber actuation in the 4-chamber module

(b) The simulated performance of one and two chambers actuation in the 3-chamber module

Figure 3.6: Results for validating the finite element simulations

2) Radial expansion constraint (sheathing) All results from the simulations of a 4-chamber module with a single chamber actuated are shown in figure 3.7a. Designs with an outer sheath achieve more bending for the same pressure. The bending of the design without a sheath drops off very quickly, which is not according to experimental results (Elsayed et al., 2014). With no sheath, the simulation could not go beyond 0.35 bar of pressure due to highly deformed elements leading to numerical instability, as a result of excessive radial expansion.

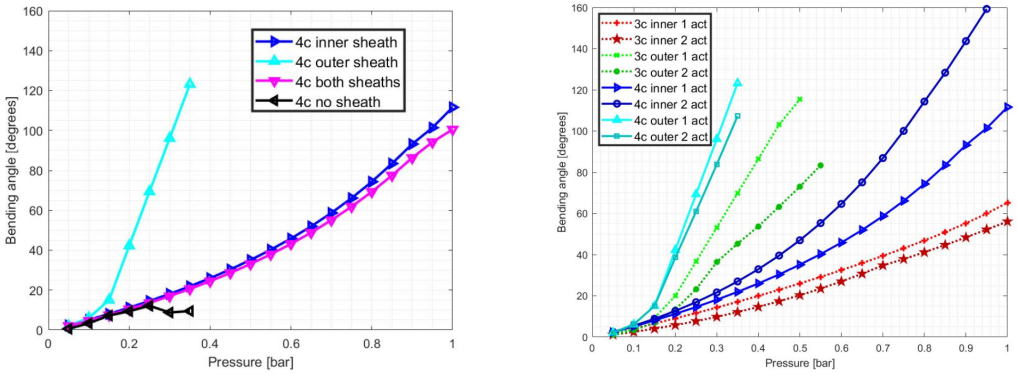

(a) The performance of the 4-chamber module with different sheathings

(b) The comparison between 3-chamber and 4-chamber modules, with different types of sheathing

Figure 3.7: Results for validating the finite element simulations

3) Number of chambers The performance curves for 3-chamber and 4-chamber modules with chamber (inner) and body (outer) sheaths were compared in figure 3.7b. The two chamber actuation results are also shown.

4) Volumetric design of pneumatic chambers The simulation results of the three volumetric designs are shown in figure 3.8. The basic design achieves more bending for the same amount of pressure. At 1 bar of pressure, the bending angles of the concave and sharp-edged designs are about half the bending angle of the basic design.

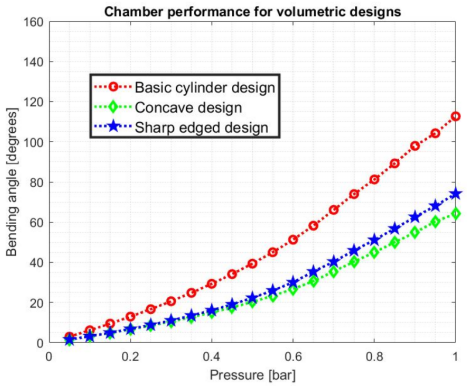

Figure 3.8: The comparison between the three different volumetric chamber designs

3.5 Discussion

In this study different design aspects in a soft endoscopic module were assessed. For this purpose, a finite element model of the endoscopic module was developed and validated against experimental measurements. Subsequently, different types of radial expansion constraints (sheathing), number of chambers, and volumetric designs of the pneumatic chambers were compared. As expected, the chambers expand inwards when only an outer sheath is used and the required pressure for the same bending is lower than when the inner sheath is used. The effect of shifting geometrical centers when only an outer sheath is used is clearly visible. The 3-chamber design with a single actuated chamber outperforms the dual chamber actuation. The performances of single and dual chamber actuation are similar in the 4-chamber design, showing that using four chambers can negate the effect of the shifting of geometrical centers.

Using both the inner sheath and the outer sheath does not result in an improvement in bending performance compared to only using the inner sheath. Using both sheaths would therefore not be beneficial, as its fabrication would be the most complex of all the designs. Using four chambers instead of three results in more bending, regardless of the type of sheath. Because all designs have the same chamber cross section diameter, the 4-chamber module cross section area has less material. It is therefore expected that this result is mostly due to the lower stiffness of the 4-chamber modules. The results of the inner sheath show that the 3-chamber design has similar bending for both the single and the dual actuated case. For the 4-chamber design, the bending for the dual actuated case is significantly higher than for the single actuated case. This was expected, due to the higher resulting moment.

Bending is more gradual using the inner sheaths. The inner sheath designs do not show the steep rise in bending at higher pressures that the outer sheath designs have. If high pressures do not pose a problem, using a 3-chamber inner sheath design would be preferred. This is because it requires less pneumatic hardware and no compensation in control is necessary when two chambers are actuated simultaneously, because the absolute value of the moment arm does not change. It could be argued that using a 3-chamber module would be preferred even

though the 4-chamber design requires less pressure for the same amount of bending, as the area per chamber can be increased more than when four chambers are used in the same size of module. This lowers the required pressure again, although more research is necessary to confirm whether similar performance can be achieved. Other advantages of using three pneumatic chambers instead of four is that more space is available for routing pneumatic tubing and that it is more suitable for downscaling the module. An example of a 3-chamber design with larger chamber cross section area compared to module cross section area is the last version of STIFF-FLOP, which has two parallel tubes per actuation chamber (Abidi et al., 2018). Because scalability is an important requirement of the soft robotic endoscope, this project will continue with the 3-chamber inner sheath design. Experiments on the achievable performance differences between the 3-chamber and 4-chamber inner sheath designs are recommended, but will not be performed in this project.

As inferred from the results of this study, the basic design outperforms the concave and sharp-edged designs in terms of pressure per degree of bending angle. Although theoretically hypothesized, experiments to confirm this would be beneficial. Since the non-basic designs require less volume, the requirements for the final endoscope determine which design parameters are more critical. If more space is required, but pressure is not an issue, chamber volumes can be made smaller without changing the basic geometry. If more space is required while the pressure has to be kept low, the volumetric design can be made to just fit the available space. This gives the maximum bending versus pressure curve within the volumetric limitations. It is expected that the concave and sharp-edged designs perform better than a basic design with a diameter equal to the smallest cross section of these non-basic designs. This study focused on chambers with equal maximum cross section areas. The volumes of the chamber designs were therefore unequal. More research is required to compare chambers with equal volume. The optimal shape can then be determined by the application requirements.

3.6 Conclusion

With the desire to find the most suitable soft endoscopic module, the combination of the methods of constraining radial expansion and the number of chambers was considered, as well as the influence of different volumetric designs. Results were obtained using finite element simulations that were validated with experiments performed in the lab and in other comparative studies.

Within the designs compared, the 3-chamber inner sheath design is the most optimal for control and pneumatic hardware requirements. The 4-chamber outer sheath design should be used if minimizing actuation pressure has the highest priority. The basic volumetric design should be used, unless other multi-module endoscope components require a trade-off in which a decreased bending performance is permitted. Further research is required to determine whether the performance of a 3-chamber inner sheath design with larger chamber cross sectional area can match the performance of a 4-chamber inner sheath design. A study on whether nonbasic volumetric designs can outperform basic designs with comparable volume should be performed as well.

Based on the endoscope requirements and the results of this theoretical study, the 3-chamber inner sheath design with basic chamber shape is chosen as the basis for the soft robotic multi-module endoscope. This is done to minimize the required hardware and calculations for control, for improved scalability. Although it is expected that the maximum bending angle of the module will be decreased, solutions to improve the bending angle again are already available. Research on the improvement of the amount of bending can be seen as a separate study, when the endoscope is closer to implementation in clinical setting. The chosen module type is suitable as the basis of the proof of concept of the soft robotic endoscope.

4 Module design and fabrication

The module design of the endoscope was chosen to have three pneumatic chambers with inner sheaths. The goal of this chapter is to finalize the design of the module based on the chosen design aspects and verify that the endoscopic module is suitable for the application. The multi-module endoscope requires that multiple modules are fabricated and that their behaviour is known and predictable so that feedforward control can be implemented.

The first part of this chapter contains the design of the module based on the study in the previous chapter. Part of the module design is the fabrication technique required for realizing the design. While some of the steps in the fabrication process could be used directly from the work of Gifari, some changes had to be made in order to include the inner sheaths. The molds were upgraded for easier fabrication as well, giving more consistent results, which in turn makes the modules suitable for physical modelling. A physical model will therefore be constructed that gives the relation between input pressures in the chambers and the resulting bending angles of the module.

This three-dimensional linear model is based on the work of Fraś et al. (Fraś et al., 2014). The working of the modules and the accuracy of the physical model will be verified by characterizing the bending angle and direction of the modules dependent on the input pressures. It was found that the physical model is not accurate in predicting the bending angle when a single chamber is actuated and that it showns a large error when two chambers are actuated simultaneously. The model is therefore expanded to better describe the behaviour of the modules. Using this model, it becomes possible to describe the behaviour of a module by determining a single parameter per chamber instead of characterizing the whole actuator range, as was done by Gifari and Jansen (Gifari, 2018; Jansen, 2018). This makes control easier to implement and lessens the impact of the fabrication differences in the pneumatic actuators.

The fabricated modules will be tested and the bending angle dependent on the input pressures will be characterized. The results are used to verify the physical model and check the design requirements.

4.1 Design

4.1.1 Dimensions

In order to focus on the multi-module endoscope design, the module design is kept close to the design of MOLLUSC, while the necessary changes based on the chosen design aspects will still be implemented. By keeping dimensions similar, a better comparison between different modules is possible as well. This means that the outer dimensions and the materials used will not be changed. The design and dimensions of the modified module are shown in figure 4.1.

Dimensions of the new module will be kept as close to the original values as possible. The main differences between the modules are the number of chambers and the method of constraining the radial expansion of the chambers. The inner thread design requires the chambers to be circular, because any non-circular chamber shape would first deform to a circle so that forces along the circumference of the chamber are equalized. The deformation of non-circular shapes would introduce unpredictable behaviour, and might lead to shifting of the geometrical centres of the chambers, which is undesired. This means that the chamber molds have changed as well.

4.1.2 Fabrication

The main part of the module, shown in figure 4.2(B), is made of Ecoflex 00-50 (Smooth on, Inc), while the top is made of the stiffer Dragon Skin 10 Fast (Smooth on, Inc). This was chosen so that the top part would deform less, resulting in a more predictable elongation of the chambers

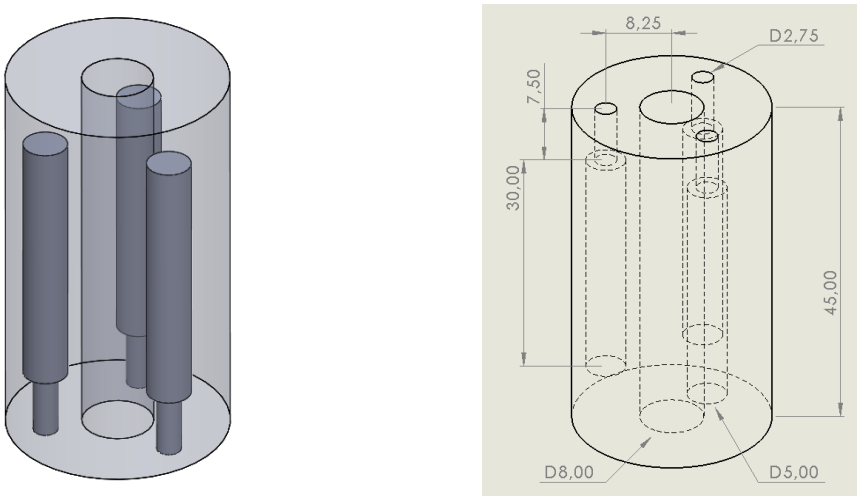

Figure 4.1: The design of the new module with inner sheath

of the module. Both materials consist of two components that have to be mixed and poured into a mold to form the module. The molds have been 3D-printed using an Object260 Connex3 using the VeroWhite and VeroClear materials (StrataSys, Ltd), which gives a smooth structure to aid in releasing the module from the mold after curing. A release agent is still used as well.

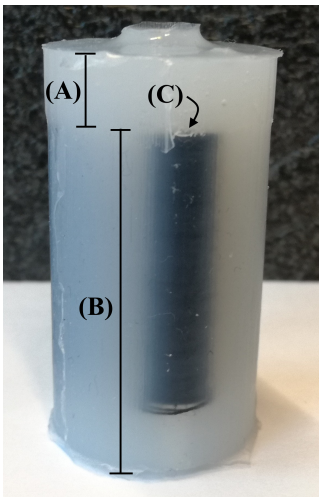

Figure 4.2: The endoscopic module with inner sheath, with (A) the top part made of Dragon Skin 10 Fast, (B) the main part made of Ecoflex 00-50, and (C) a chamber with internal thread (sheathing) that prevents radial expansion of the pneumatic chambers.

The inner sheath module design required modifications to the molds and the production steps. The inner sheath is made from standard sewing thread. To embed the thread, a thin layer of 0.5mm of Ecoflex 00-50 is poured in a seperate mold first (as was also done by Fraś et al. (Fraś et al., 2015)). The molds for this step are shown in figures 4.3a and 4.3b. After curing, the thread is wound around the chamber molds with the material. This thin layer prevents the thread from unraveling when the chamber molds are removed and when the chambers are pressurized. Care was taken to completely cover the layer of Ecoflex to prevent expansion of material between holes in the coverage, which risks rupturing the material due to large strain.

In the second step of the process, the threaded chambers are placed in the main module mold, which is shown in figure 4.3c. This mold also holds the central cylinder and is capped off by a funnel for the Ecoflex mixture that serves in positioning the chamber molds as well. Ecoflex

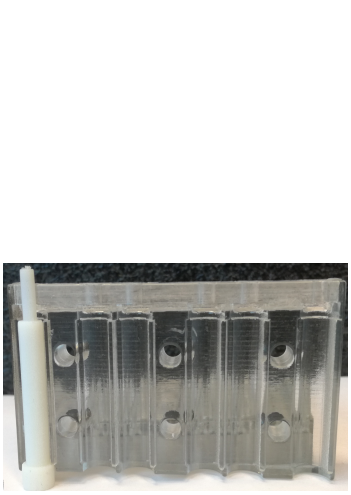

(a) The mold for creating a 0.5mm thick layer of Ecoflex around the pneumatic chambers (open)

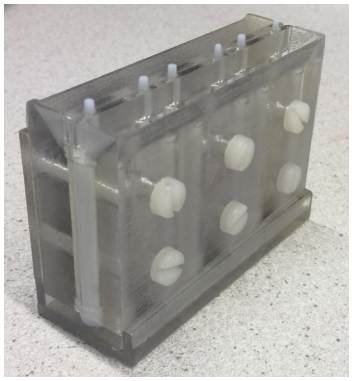

(b) The mold for creating a 0.5mm thick layer of Ecoflex around the pneumatic chambers (closed)

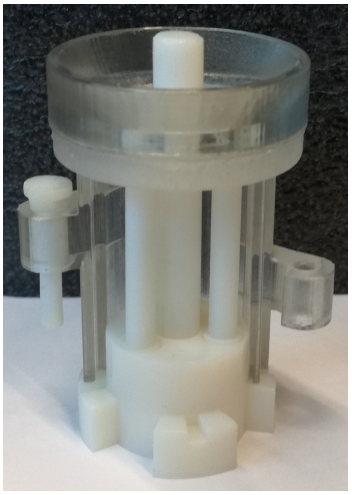

(c) The mold for creating the endoscopic modules with inner thread (open)

Figure 4.3: The molds for creating the endoscopic modules

00-50 is then poured to finish the main part of the module. After the required curing time, the main part of the module is taken from the mold and the chamber molds are carefully removed. The module is rotated in the third step and new chamber molds, that are easier to remove via the smaller holes, are placed via the other side of the module. The main mold is reconfigured for the final length of the module and the mixing and pouring steps are repeated with Dragon Skin 10 Fast. When this material is cured as well, the basic endoscopic module is finished and the molds can be completely removed. Each new module is tested with air pressure up to 1 bar to check for leaks or deformations that could lead to rupture of the material.

4.2 Physical model

Fraś et al. (Fraś et al., 2014) describe a physical model for determining the bending angles of the STIFF-FLOP module for both the unloaded and the loaded cases based on the constant curvature assumption. The model takes the force on every cross section of the module, that is dependent on the applied pressure times the chamber crossectional area, and calculates the moment and force that bend and elongate the module. By summing all infinitessimal angles over the whole length and elongation of the module, the final bending angle is obtained. Because the moments are vectors, it is also possible to calculate the bending direction, although this is not directly demonstrated. That the model can be used for determining the three dimensional configuration, is demonstrated however. The relation between the theoretical model and experimental data is not shown.

The most important equations of the physical model show the relations between the applied pressure and the resulting bending angle dependent on the module's properties. Due to the forces in the longitudinal direction of the chambers, the module elongates with Δl and has a curvature κ. This is represented in equations 4.1 and 4.2. The bending angle of a module is then the summation of the curvature over the final length of the module, shown in equation 4.3. The bending direction of the module is determined by the moment arm, which is the result of the combination of forces of the three chambers.

$$\Delta l = \int_0^{l_0} \Delta dl = \int_0^{l_0} \frac{F_p}{AE} dl \tag{4.1}$$

dl: length of a slice of the module, F_p: the force due to the pressure times the chamber cross sectional area, A: the area of the cross section of the module that is not part of the chambers (so the module's material) (Fraś et al., 2014).

$$\kappa = \frac{1}{\rho} = \frac{M}{EI} \tag{4.2}$$

κ: the curvature at a slice of the module, ρ: curvature radius, M: moment due to the chamber pressure times chamber cross sectional area times the moment arm, I: the second moment of area of the slice of the module (Fraś et al., 2014).

$$\alpha = \int_0^{l_0+\Delta l} \frac{1}{\rho} dl \tag{4.3}$$

α: the total bending angle of the module, l_0: the initial length of the module, Δl: the extra length of the module due to the total actuation force, dl: the length of an infinitessimal slice of the module (Fraś et al., 2014).

4.2.1 Implementation

This physical model is implemented in Matlab (MathWorks) and used to predict the bending angle and direction of the endoscopic module. Appendix B shows the steps required for calculating the bending angle and direction from the pressures applied to the three chambers. Using the Young's modules of Ecoflex 00-50 equal to its 100% modulus of 12psi, or 82737.1 Pascal, (Smooth-On, Inc) the bending angles and directions are plotted for different maximum pressures from 0.1 bar to 1 bar by varying the chamber pressures linearly. The chamber pressures were chosen in such a way that the bending direction of the module would trace 360°. This was done by always having at least 1 chamber at maximum pressure, while varying one of the other chambers. The resulting actuator space is shown in figure 4.4.

As can be seen, a hexagonal figure is traced by always setting one of the chambers at maximum pressure. The six corners are the points of single or dual chamber actuation at maximum pressure. It is clear that the amplitude (which is the bending angle) of these points is not equal. Dual chamber actuation gives a slightly larger bending angle compared to single chamber actuation. This was found by the study in chapter 3 as well.

The reason for this larger angle is directly clear from the model. By actuating two chambers simultaneously, the amplitude of the moment arm is equal to the case with single chamber actuation, but the elongation of the module is larger. The model assumes constant curvature, which means that the curvature of the module is the same over the whole length of the module. The model determines this curvature using the moment arm and integrates this bending depending on the moment arm over the total length of the module. This determines the angle of the end face of the module, or the bending angle. A longer module has a higher bending angle with the same moment arm.

Although a model can be used to predict the bending of the module under defined chamber pressures, it is necessary to verify this model and to compensate and alter the model for any deviations that might occur in an actual endoscopic module. This is why the pressure versus bending angle curve of the fabricated modules will be characterized.

4.3 Characterization

Knowledge is required of the bending angle of the module at the applied pressures in order to apply feedforward control. For this the bending angle dependent on the applied pressures has to be characterized. This characterization can then be used to validate the static model and fill in the physical parameters.

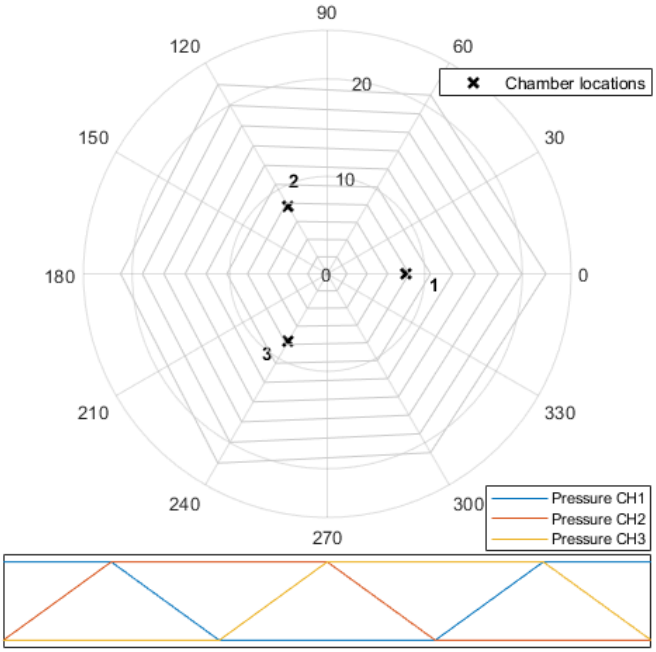

Figure 4.4: Bending angle and direction based on the applied chambers pressures, based on the physical model. The main plot axes contain circles of equal amount of bending, while the bending direction is shown in 2D. The locations of the pneumatic chambers are shown (not to scale). The pattern of applied pressures is shown in the subplot. Each pattern is scaled with a maximum amount of pressure (ranging from 0.1 bar to 1 bar) and every closed hexagonal shape is linked to one of these maximum pressure values.

4.3.1 Method

Characterization of the modules is performed using a setup consisting of pressure regulators from Festo and an Aurora Electromagnetic (EM) tracker (NDI Medical). The EM tracker is used to measure the bending angle of the module and outputs the six DOF position and orientation of the sensor that is placed on the tip of the module. The rotation output of the tracker with a 6 DOF sensor is in quaternions with an accuracy of 0.55° (NDI, 2019). Matlab is used to transform the quaternions to rotation matrices.

For every module all individual chambers and all combinations of two chambers will be characterized. During a measurement the pressure of the chamber(s) is increased in steps of 0.05 bar and the actual value is read back via the feedback signal of the pressure regulator. This feedback signal is accurate within 2% of the full scale value, or within 40mbar. Data is synchronized by timing this increase in pressure with the number of the measurement frame of the EM tracker, which measures 40 frames per second. Every 5000 frames the pressure is increased and the data is picked exactly from the middle of a set of 5000 points with the same pressure.

A script was written to convert the quaternions from the measurements to rotation angles and the initial position at the start of the measurement is removed from all samples. The relative angle of every measurement is then known. The eigenvectors and values of the resulting rotation matrix contain the axis of rotation and the rotation angles. This is represented in figure 4.5. The absolute rotation angles of the module are therefore determined by finding the angle of the complex eigenvalues of the rotation matrices.

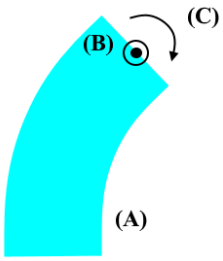

Figure 4.5: Schematic representation of the values that are measured using the EM tracker and that are used in calculating the bending angle of the module for the applied pressures. (A) is the module, (B) is the axis of rotation that is perpendicular to the field of view, and (C) is the rotation angle represented by the angle of the complex eigenvalues of the rotation matrix.

Next to the characterization of the amount of bending, the bending direction for the combination of two chambers with different input pressures will be measured as well. This will be done using two pressure regulators and varying the pressures in both chambers from 0 bar to 1 bar in steps of 0.25 bar. The bending direction is a vector perpendicular to the bending axis that is found, projected onto the table on which the module stands. For processing the data, all bending directions are defined relative to the bending direction of the module when only one of the chambers is actuated with 1 bar of pressure. Three sets of measurements will be performed, one for every pair of chambers.

4.3.2 Results

The results of three endoscopic modules are shown in figure 4.6 together with the predictions of the physical model.

It can be seen that bending of the modules is close to linear, but that the lines curve upwards. By combining the graphs in a single figure, it is directly clear that repeatability between modules is achieved. The maximum difference between chambers of different modules is 10% for single chamber actuation and 13% for dual chamber actuation. The differences between chambers within the same module lie within 4% and 8%, for single chamber and dual chamber actuation respectively.

Dual chamber actuation gives higher bending angles than single chamber actuation, as was expected. The single chamber maximum bending angle at 1 bar is close to 25°. It is also clear that the physical model cannot be used to represent the modules, as the model has an error of at least 4° at 1 bar of input pressure, with a maximum error of 11° in case of dual chamber actuation.

Figure 4.7 shows the characterization of the combination of two pneumatic chambers at independent input pressures. A shape resembling a hexagon can be seen, which is in accordance with the expected values from the model. There seems to be a large measurement error in this figure, as similar input pressures for the same chamber give different results in separate experiments and the angle between two tested chambers does not reach the expected 120° in any of the measurements. The difference in results between separate measurements might suggest that the behaviour of a chamber is not repeatable, but repeated characterization of the same chamber is required to determine this. The repeatability between different chambers, and even between modules, suggests that a problem within the measurement setup is a more likely cause of the differences.

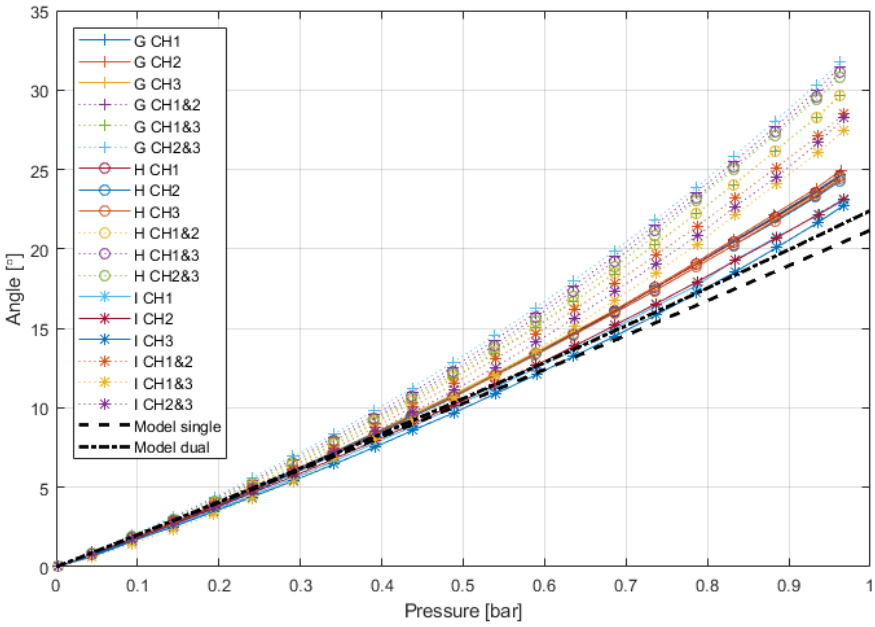

Figure 4.6: Bending angle dependent on chamber pressures for the modules 3G, 3H and 3I for single chamber (CHi) and dual chamber actuation (CHi&j). The calculated bending angle using the static model from literature is shown as well.

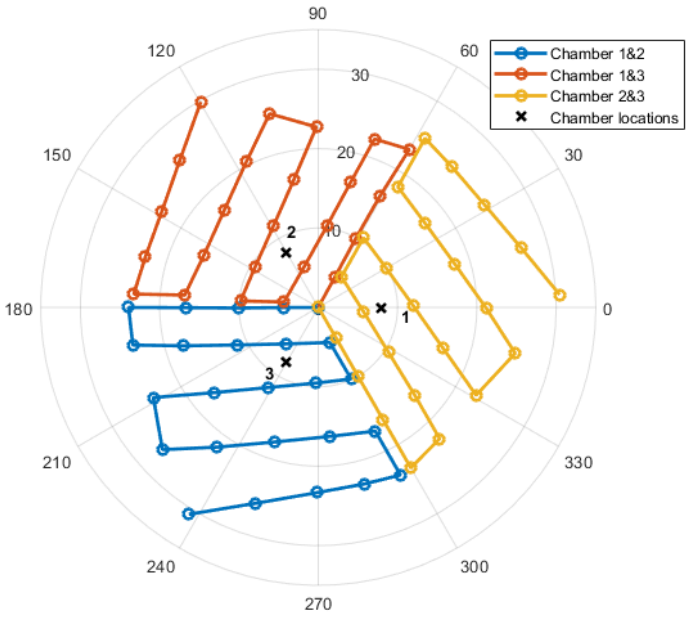

Figure 4.7: The characterization of the bending angles and directions of a module, with the direction shown in the 2D plane and the bending angle as the amplitude. Three pairs of chambers were characterized and the locations of the chambers are shown (not to scale). Both chambers in a pair were actuated with 0, 0.25, 0.5, 0.75, and 1 bar of pressure. The data points are the results of all combinations of these pressures in the two chambers.

4.4 Improving the physical model

The bending angle versus input pressure characterization of several modules shows that the model works well for lower pressures, but does not describe the behaviour well for input pressures above 0.5 bar. The reason that the bending angle curve increases more with dual chamber actuation, is that the elongation of the module increases this angle as well. The bending angle of the module is the curvature summed over the module's length. Dual chamber actuation elongates the module more than single chamber actuation and this adds to the resulting bending angle.

The increase in length due to elongation does not seem to be enough to explain the difference in bending angles between the model and reality. While the bending is dependent on geometry and the Young's modulus of Ecoflex 00-50, only changing the Young's modulus to fit the model to the data does not give the desired results. Modelling a material that is less stiff results in higher bending angles overall, but to achieve the measured angles for dual chamber actuation, the predicted angles for single chamber actuation become too high.

It is therefore expected that the modelling error does not lie in the material properties, but in the geometry of the module. When the module elongates, a decrease in diameter can be observed. This decrease in diameter will decrease the second moment of area of the module, which influences the module curvature. For a uniform deformation, the relation between elongation and decrease in diameter can be captured in a material's Poisson ratio. Finding this ratio for Ecoflex 00-50, combined with the fact that the module's second moment of area scales with r^4, should make it possible to improve the physical model.

This does not hold for the endoscopic modules, however, because their outer diameter is fixed at the connector pieces. This means that the change in diameter of the module is not uniform over its length and that a Poisson ratio cannot be used. In order to improve the model, several scaling factors for the second moment of area were therefore tried until the predicted and measured bending angles matched at 1 bar of input pressure.

It was found that the second moment of area should be scaled by $(\frac{l_0}{l_0+\Delta l})^3$, or the inverse of the elongation cubed, to give the correct results. This change in the second moment of area based on the elongation of the module is therefore added to the model. The results of the characterization combined with the results of the improved model can be seen in figure 4.8 and 4.9. The model is now able to predict the bending within an error of 2°, which is under 8%, over the whole actuator range. The improved model of the actuation range based on constant maximum pressure, as was plotted in figure 4.4, can be seen in figure 4.10.

4.5 Discussion

4.5.1 The endoscopic module

A new module with three pneumatic chambers using the inner sheath was realized and characterized. The characterization of different modules shows that the behaviour is repeatable. The maximum bending angle at 1 bar was found to be around 25° for single chamber actuation and 31° for dual chamber actuation. This is lower than the 40° set by the module requirements and lower than expected from the simulation results in chapter 3. The reasons that the module did not bend as far as was expected from simulation is expected to be due to the shape, and consequently cross sectional area, of the chambers. The simulations were performed with halfcircular chambers, and with circular chambers with a larger diameter. The general shape of the pressure versus bending curve of the measurements show similar behaviour, which means that the values of the bending angles might be scaled with the chamber area. More research is required in order to determine why the actual bending angles are lower. This will help in improving the finite element models. With reliable finite element models, the fabrication of new prototypes can be postponed until after desired results are obtained in simulations. Because

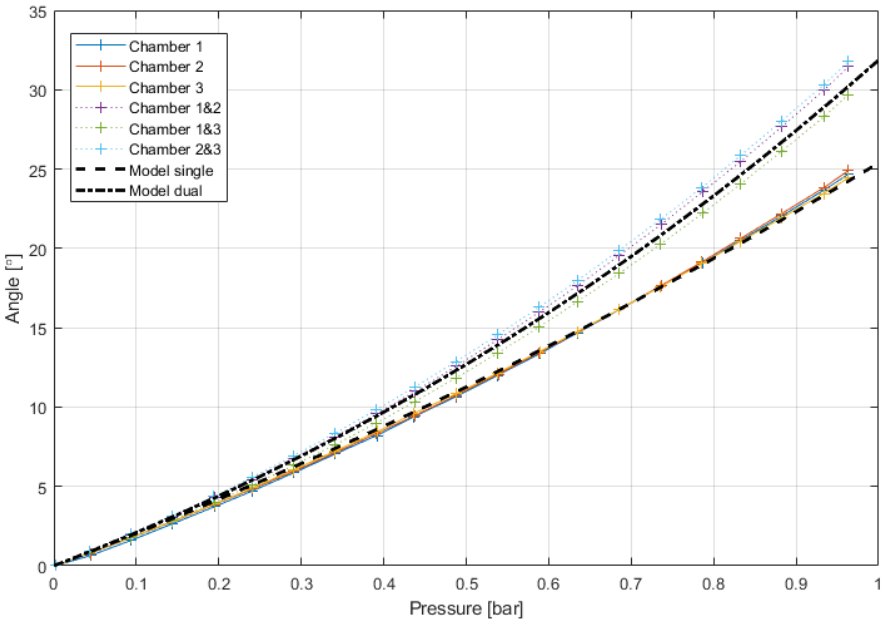

Figure 4.8: Bending angle dependent on chamber pressures for the module 3G for single chamber (CHi) and dual chamber (CHi&j) actuation, together with the improved physical model.

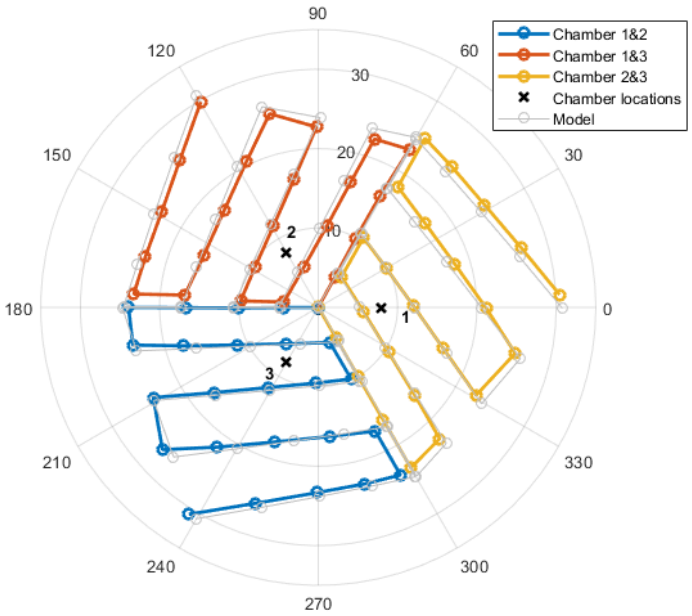

Figure 4.9: The characterization of the bending angles and directions of a module with the predictions of the model overlayed. The direction is shown in the 2D plane and the bending angle is shown as the amplitude. The data is equal to the data of figure 4.7.

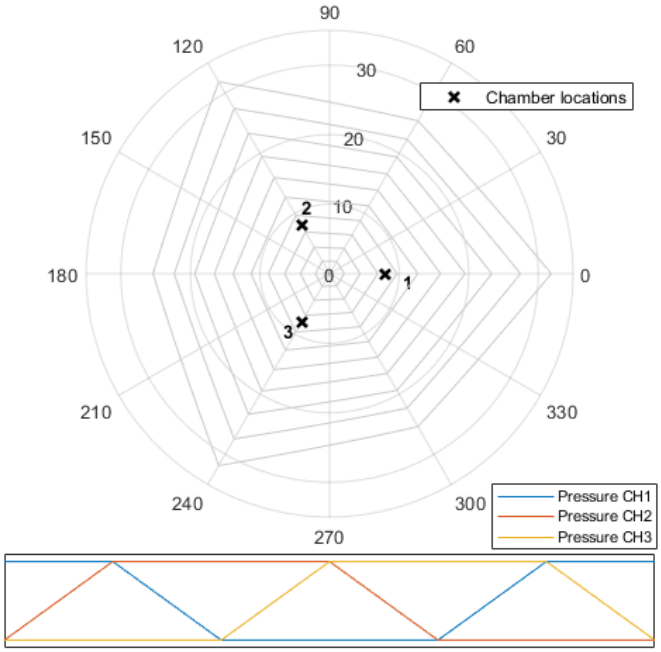

Figure 4.10: Bending angle and direction based on the applied chamber pressures, with the updated physical model. The main plot axes contain circles of equal amount of bending, while the bending direction is shown in 2D. The locations of the pneumatic chambers are shown (not to scale). The pattern of applied pressures is shown in the subplot. Each pattern is scaled with a maximum amount of pressure (ranging from 0.1 bar to 1 bar) and every closed hexagonal shape is linked to one of these maximum pressure values.

simulations are much faster than fabrication, this will aid in faster prototyping of new modules with different dimensions.

The maximum bending angle of the realized modules is expected to improve by using larger pneumatic chambers, material that is less stiff, and by allowing higher maximum pressures. Not all of this can be directly implemented because of fabrication limitations. More research is required towards modules with higher bending angles.

4.5.2 The physical model

The improved model can be used to predict the bending of a module with inner sheath under known chamber pressures, but it also contains implicit assumptions about the different aspects of the module. The static model assumes constant chamber cross sectional area, which means it cannot be used to predict the bending of the outer sheath modules. Modelling the modules with outer sheath would require compensation for the force on the chamber crossectional area based on the applied pressure. Because the radial expansion is still constrained by the outer sheath, which introduces non-linearities, as discussed by Gifari and Fraś et al. (Gifari, 2018; Fraś et al., 2015), more knowledge about the orientation of the module and the size of the other pneumatic chambers is required for this compensation. This means that the inner sheath module requires a simpler model than the outer sheath module.

The linearity and repeatability of the module with inner sheath, in terms of bending and of multi-chamber actuation, are an advantage for the control. A completely predictable module means that any requirements in terms of bending can be directly translated to module dimen-

sions and actuation pressures. It should be noted that the model does not take external loads into account, which might have a significant influence on the relation between pressure and bending. Without any external disturbances, the module is steerable with an error of 13% at most, if differences due to fabrication are not compensated for. If the model is extended to take individual chamber behaviour into account, based on characterization, this number can be improved significantly.

The physical model was improved compared to the model used by Fraś et al. (Fraś et al., 2014) by decreasing the second moment of area of the module, I, based on the elongation. The second moment of area was scaled by the change in length to the third power, but no clear reason for this third power is known at the moment. The second moment of area scales with the module radius to the power of 4, which means that this, in combination with the Poisson ratio of Ecoflex 00-50, could have been used to predict the correct amount of bending. Because using a the fourth power did not give correct results for both the single chamber actuation, as the dual chamber actuation, it was already hypothesized that the Poisson ratio could not be used due to the non-uniform deformation of the modules.

It is also unclear whether the second moment of area can be changed independently of the Young's modulus of the material. It is possible that the stiffness of the material changes for significant elongation, especially when looking at the curvature. In the current model, this stiffness is considered constant and only the geometry of the model is changed.

A better approach for improving the model would be to better characterize the change in bending angle based on the elongation and couple this to a new parameter. This parameter could also be used to describe the differences in behaviour that were seen between different modules. More research is required to determine the exact cause of the increased bending angle for more elongated modules. This could help in determining the relation between the elongation and the second moment of area or the relation between the elongation and the bending stiffness of the module. This would result in a more physical description of the module. This is however not necessary for control, because a simpler (but more time consuming) characterization can be used as well.

The elongation of the modules under bending was never actually measured. This means that it could still be possible that a different effect is responsible for the errors in the expected bending angle. While a significant decrease in the module's diameter was observed, it is not ruled out that elongation has an insignificant effect on the bending angle of the modules (outside of the effects described by the original physical model). Experiments should therefore be performed to validate that the elongation influences the bending significantly.

The physical model also assumes that the moment arm that causes bending is dependent on the distances between the chambers and the centre of the module. Although this seems a correct assumption when the results of the model and the actual module are compared, this does not necessarily have to be correct. The centre of the module is not fixed, which means that it does not have to be the joint. Because the model made usable predictions after the addition of the change in second moment of area, this was not looked into. More research could be beneficial if a deeper understanding of the behaviour of the module is desired.

4.6 Conclusion

3-chamber inner sheath modules were fabricated and their bending performance was characterized. Based on the results, the static physical model of the modules was improved to better account for the higher increase in bending angles at higher input pressures. The module's behaviour turned out to be repeatable and close to linear. The maximum bending angle of the module with the required dimensions was 25° for single chamber actuation, which means that the bending angle requirements of the module were not met. Actuating different chambers

gives results that are not dependent on actuation order, which is an improvement on the behaviour of MOLLUSC. This means that the physical model can be used in feedforward control of the module and that any angle that lies within the limits of the allowable pressures can be reached.

A predictable module aids in the design of the multi-module endoscope, because application requirements can directly set the requirements for the individual modules. Even though it is already expected that feedback is required for steering the endoscope along paths, the path planning algorithms could benefit from the constant relations between pressure and bending angle. With a predicable module, only external factors and fabrication accuracy will introduce disturbances in control.

Now that the endoscopic module and its behaviour under different chamber pressures have been defined, the next step is controlling the pneumatic chamber pressures in order to achieve the bending angles required by the setpoints. The next chapter will look at the practical requirements for controlling the individual modules and introduces the hardware and software that is used for steering the soft robotic endoscope.

5 Steering the endoscopic modules

The physical model of the endoscopic module can be used to calculate the required chamber pressures for a desired module bending angle and direction. The pressures in the pneumatic chambers have to be set precisely in order for the module to bend according to the desired setpoint. In controlling the soft robotic endoscope, all pneumatic chambers of all modules require precise control of the applied pressure.

This chapter will look at what is required for steering the endoscopic modules and will create the basis for control of the multi-module endoscope. A concept design of the system hardware for controlling the soft robotic endoscope will be created. The hardware consists of pressure regulators that require an analog voltage for setting the pressure setpoint and a main supply of high pressure air. Setpoints per pneumatic chamber can be set by software, which is designed to include the model of the endoscopic modules in order to directly set the pressure setpoints based on the required bending angle and direction. The interface between the software and the pressure regulator will be designed and tests will be performed to assess performance.

The first steps towards a multi-module endoscope are made with the design of the hardware and software for controlling the endoscopic modules. By making sure that the translation between required bending angles and required chamber pressures is done in software, this software can be used to steer the complete endoscope when a position configuration (or path) is determined.

5.1 Analysis

Based on the requirements for the dynamics and control, the soft robotic endoscope should have several degrees of freedom and should be able to follow a predetermined path. This means that the configuration of the robot along its whole length can be controlled. The endoscope will have feedforward control, so a relation between bending angle and input pressures is required.

Using the relation between bending angle and input pressures, a path can directly be translated into pressure setpoints for the pneumatic chambers. Following a path might be a matter of changing these setpoints in time, but may include the dynamics of the system as well.

5.1.1 Required response time and accuracy

The required response time of the system is dependent on the application. In MIS and NOTES response times have to be in the order of seconds. The pressure regulators used in characterization can support a flow of up to half a liter per second and the volume of the pneumatic chambers is less than a milliliter. The response time of the pressure regulators used in characterization are therefore in the order of milliseconds, which is sufficient.

Because one of the requirements of the endoscope is MR-compatibility, the pneumatic hardware that works electrically, such as the pressure regulators, has to be placed outside of the MRI room or with enough distance from the MRI bore (further than 6 meters). Pneumatic tubes running from the pressure regulators to the endoscope therefore have lengths in the order of meters. This has significant influence on the response time of the pneumatic system. The system can be represented as a storage of momentum of air in series with a resistance to flow and a storage of air pressure, which is of second order. A sufficiently fast response time of the pressure regulators might lead to overshoot of the pressure inside the pneumatic chambers, or an unstable situation, due to the inertia of the air in the tube. This might lead to discomfort or even damage to the endoscope.

Because the pressure regulators used have a fixed response time and are meant for specific applications, the pneumatic tubing will be kept short to decrease the risk of overshoot of pressure.

Modelling of the pneumatic tubing and the required flow will help in ensuring stability, but this will not be done in this project, as it also requires hardware of which the response time can be tuned to the system. Of course, response times may be lowered in software as well. This will be left as a recommendation for further research, because the problem only starts to exist when the length of the pressure tubes becomes too long. This will not be the case in the setup in this project.

5.2 Design

The chamber pressure is regulated using pneumatic pressure regulators (Festo) which connect between the main pressure lines in the lab and the chambers. The pressure regulators give feedback on the achieved pressure, but contain an internal controller to regulate the pressure as well. An electronic signal is required for setting the pressure setpoint. This means that when the desired pressure is known, the setpoint for the regulator can be calculated and the correct voltage can be applied to the input of the regulator.

Setting the voltage is done via the pulse width modulated (PWM) output of an Arduino UNO connected to a laptop with Matlab. Using the available Arduino libraries it is possible to run a script in Matlab that directly sets the output pressure setpoints of the regulators using PWM. This PWM output voltage has to be filtered and the pressure regulators require a signal between 0V and 10V, of which the Arduino can only provide the first half, up to 5V. This is why extra electronic hardware has to be designed in order to utilize the whole output pressure range.

5.2.1 Pneumatic driver shield

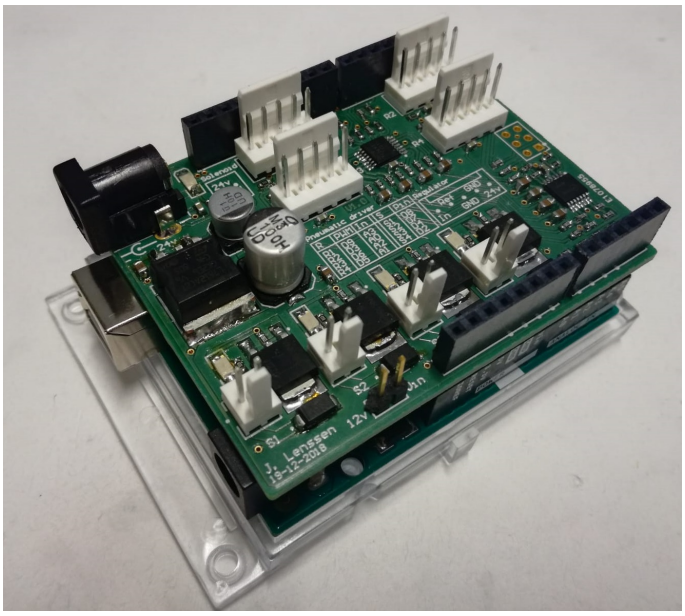

Figure 5.1: The Pneumatic Driver Shield

In order to make use of the simple interface that the Arduino provides for setting the chamber pressures, a pneumatic driver shield printed circuit board (PCB) was designed that aids in translating the PWM output of the Arduino to an analog voltage in the range suitable for the pressure regulator. The PCB of the driver shield has the shape of the Arduino and can be placed directly on the Arduino board itself. This helps limiting the number of cables and makes the setup more robust. The driver shield was designed to be generally applicable, meaning that not all design choices are necessarily made for the multi-module endoscope.

Can control four pressure regulators
Can control four solenoid valves
Has a response time in the order of 10's of milliseconds
Has a maximum deviation of 5% in its output value
Can read the pressure feedback from the regulators
Can provide power to the Arduino UNO
Can be used in combination with other shields or extensions
Is self contained, so no extra documentation or hardware is required

Table 5.1: Requirements for the electrical design of the pneumatic driver shield

Based on the available board space, the number of PWM outputs and analog inputs of the Arduino UNO, and the requirement to be generally applicable, the design choices in table 5.1 were made for the pneumatic driver shield.

The PWM filter is based on a ripple filter by Woodward (Woodward, 2017), that provides fast response time and low ripple. The output of the Arduino is amplified by a factor of two using a basic operational amplifier (Op-amp) to reach the required voltage range. The filter was verified in simulation using LTspice IV (Linear Technology) using the design in figure 5.2. The feedback from the pressure regulators is read back via a resistive divider that connects to the analog inputs of the Arduino. The solenoid valves are switched using a suitable transistor and flyback diode, comparable to what was used by Gifari (Gifari, 2018). LEDs indicate the status of the solenoid valves and the status of the input supply voltage. The whole circuit is fed from 24V. A linear voltage regulator that ouputs 12V is added in order to be able to feed the Arduino from the same supply as well for stand-alone applications. This 12V supply can be used by placing a jumper connector on the header shown in figure 5.3(D).

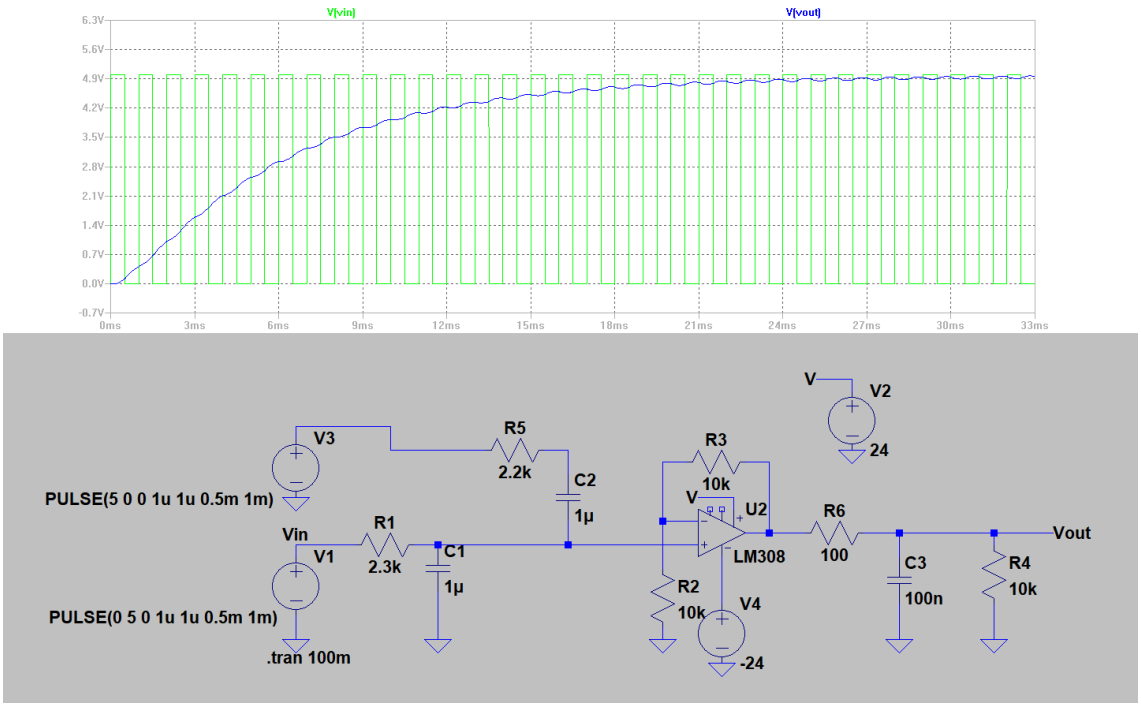

Figure 5.2: Schematic representation of the PWM filter and amplifier for creating the voltage reference for the pressure regulator based on the output of the Arduino. This filter requires the inverse of the PWM signal as well. The filter settles in 30ms and has a ripple of less than 70mV, or less than 0.7% of the full scale output voltage.

The designed PWM filter was tested on a breadboard and performed as was expected from simulation. The PCB was therefore fabricated according to the schematics. All tests showed that the final PCB was completely functional. The pneumatic driver shield can be seen in figure 5.1. A description of the layout of the shield is given in figure 5.3.

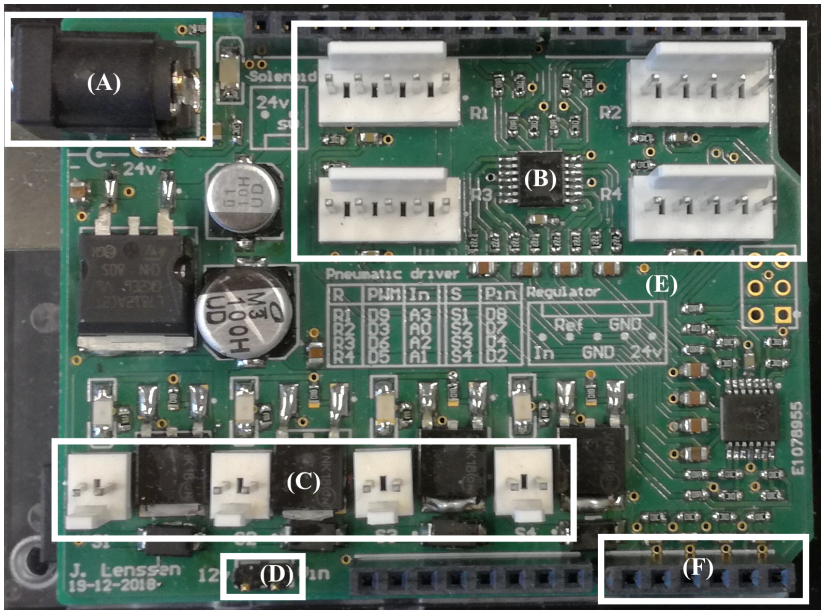

Figure 5.3: The Pneumatic Driver Shield, with (A) the DC input for connecting the 24V power supply, (B) the connectors for connecting four pressure regulators Ri, (C) the connectors for connecting four solenoid valves Si, (D) the jumper that determines whether the Arduino UNO is powered from a separate source or not, (E) the pin numbering information required for connecting the hardware, and (F) the (auxiliary) analog inputs Ai.

5.2.2 Matlab app

Using Matlab's Appdesigner an app was written that can be used for setting the desired chamber pressures using the pneumatic driver shield and the Arduino via a user interface (UI). The combination of the driver shield and the app make modifying a test setup something that can be done in minutes. Figure 5.4 shows the UI of the app.

While the UI of the app is universal and can be used to directly control the solenoid valves and regulators manually, the app also contains background routines that aid in the control of multiple valves and regulators in parallel or sequence. An array of setpoints for the regulators and solenoid valves can be defined, with values changing every step, and the app will step through the values and set the hardware accordingly.

The implementation of the model of the actuator is included and adds a layer that translates between required bending angles and hardware setpoints. This makes it possible to let the actuators follow a predetermined path. Precise timing is not implemented, due to unpredictable delays in the communication between Matlab and the Arduino via USB. The app serves as a demonstration of the capabilities of the endoscope. Manual control of each individual regulator or solenoid valve is not desired in the final application. Instead, control software that is written specifically for the final application will require bending angle and direction setpoints per module, which in turn might be the result of path planning software requiring the environment and goals of the surgery tasks. The path planning problem for the soft robotic endoscope is being solved by another student at RaM (J.W. Lageveen). Software for the final application

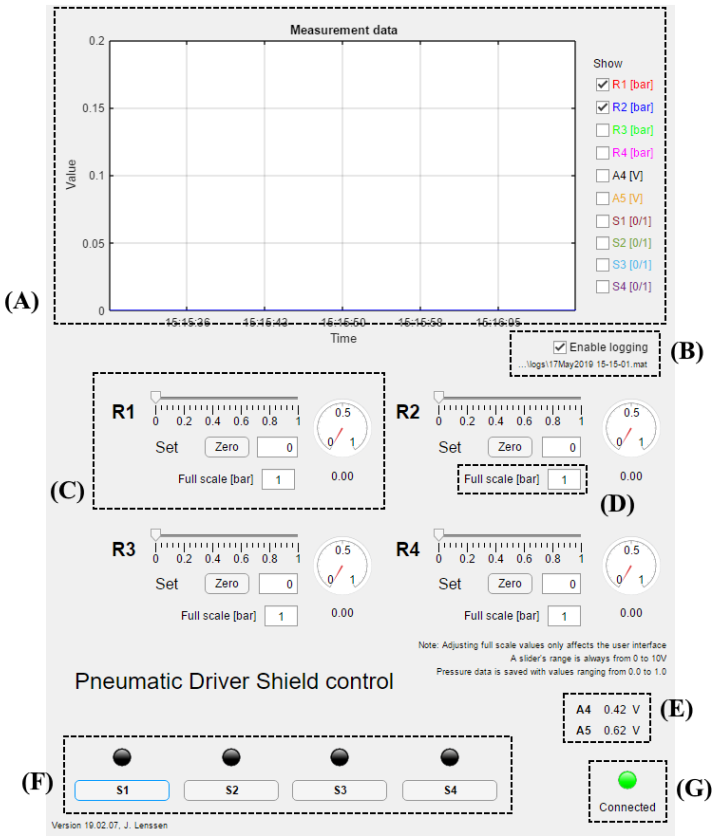

Figure 5.4: The User Interface for using the pneumatic driver shield, with (A) the plotted measured data for the selected inputs (feedback from regulator Ri, analog input Ai, or the state of solenoid valve Si), (B) the controls for saving the measured data in a log file, (C) the controls for, and feedback from, a single pressure regulator Ri, (D) the edit field for setting the full scale pressure of the pressure regulator that is used, (E) the measured values of the auxiliary analog inputs Ai, (F) the buttons for setting the state of the solenoid valves Si, and (G) the indicator for showing whether or not an Arduino UNO has been connected. The labels correspond to the labels on the PCB of the pneumatic driver shield.

is not written as part of this project, as this is necessary when the endoscope is closer to being used in clinical practice.

5.3 Results and discussion

Software and hardware were tested with the endoscopic modules. With the possibility of setting four separate pressure regulators, all chambers of the module could be pressurized independently. The control of four solenoid valves also made it possible to test and characterize the designs of chapter 7, which will follow. The ability to log all measurements made it possible to save the results of all measurements, although the delay in the connection between the Arduino and Matlab did not permit high resolution measurements. About 6 sets of samples per second could be saved, which is sufficient for static measurements of the bending of the modules, but does not give enough details for measuring with timescales below a second.

Control of different pieces of hardware simultaneously (multiple pressure regulators for example) suffers from the same delay, which limits the speed with which the endoscope can switch between states. A different method is needed if more frequent datapoints are required. As all inputs are saved in every measurement in the log file, efficiency can be improved by excluding datapoints from inputs that are not needed. The app was, however, not designed as a data logger. Its primary function is being able to easily set the required pressures and solenoid valve

states and this goal was achieved. The logging function helps in static measurements and can be used to reconstruct experiments.

The inverse model of the endoscopic module was implemented and gave the expected chamber pressures based on the required bending angle and direction. The accuracy of the model was already treated in chapter 4.

5.4 Conclusion

A control system was designed for controlling the bending angle and direction of a single endoscopic module based on a physical model. The hardware and software developed made it possible to do the static measurements required for characterizing parts of the endoscope. Integrated routines added the ability to step through configurations and the inverse static model enabled the user to directly set the desired bending angle and direction in the software. The software forms a suitable basis for the control of a multi-module endoscope, although the delay in communication between software and the Arduino might become an issue when fast responses are necessary.

6 The steerable multi-module endoscope

This chapter will treat the design, fabrication and control of the multi-module endoscope system based on the new module design. Using the new chamber design and continuing with the general hardware of the pneumatic driver shield, a steerable robotic endoscope will be realized consisting of three pneumatic actuator modules.

The endoscope will be designed according to the set requirements, although scalability is still left open for improvement. An analysis on the robot kinematics and the effects on the control system will be performed. The results are used in the fabrication of the endoscope and especially in the design of the connecting elements between the endoscopic modules. Three modules are stacked in order to create the multi-module endoscope. The relation between bending angle versus chamber pressure of each module is known. The endoscope is controlled using the Matlab app and multiple pneumatic driver shields. The performance of the endoscope will be verified by comparing the bending angles of the modules with the expected values. It is expected that the endoscope cannot reach its whole theoretical range, because the modules have been characterized without any load and the weight of the endoscope will influence the bending behaviour of the modules.

6.1 Analysis

6.1.1 Multi-module kinematics

Control of the multi-module endoscope is based on constant curvature kinematics, as explained in chapter 2. The relevant transformations for the multi-module endscope are the specific mapping and its inverse between the configuration space containing the arc parameters and the actuator space containing the pneumatic chamber pressures. The independent mapping between the task space containing the orientation of the endoscope and the configuration space is solved by Webster and Jones (Webster III and Jones, 2010).

The mapping between the arc parameters (constant curvature approximation) and the chamber pressures was already solved by the model of the pneumatic actuator in chapter 4. This means that, as soon as the required position and orientation of all the modules are known, the required chamber pressures of all modules can be calculated and applied.

6.1.2 Pneumatics

As the name implies, the multi-module endoscope is built up from multiple individual modules. The modules have to be connected in series so that a long, steerable tube is created through which surgical instruments can be guided. Hollow tubes have to be routed through the endoscope that connect the pressure regulators to the pneumatic chambers. These pneumatic tubes are stiff and have a lot of influence on the bending of the modules. The original STIFF-FLOP design (Cianchetti et al., 2014) routes these tubes through the chambers of the modules and applies folding in order to reduce the impact of the tubing. The 3-module endoscope contains nine tubes that all have to be routed through the first module. While many options are available for routing, the concept is not scalable. Endoscopes with more than three modules require more tubes, which take up more space inside the modules. Although tubes with smaller diameters can be chosen, there is a limit, either in terms of available sizes, or in terms of possible flow. Smaller tubes restrict the flow required for actuating the module and make the system slower by increasing the time constant for pressurizing a chamber. A more scalable solution is required.

6.2 Design

Because scalability of the endoscope is an issue treated in a separate chapter, namely chapter 7, the tubing for the multi-module endoscope will first be routed outside of the modules. This is reflected in the design of the connector pieces between the modules, that connect the tubing to the chambers of the modules. Routing the tubing outside of the module does not directly affect the control, although it will affect the stiffness of the endoscope and might introduce disturbances.

6.2.1 Connector pieces

The endoscopic modules are connected via 3D-printed connector pieces that contain channels for connecting the pneumatic tubing to the chambers of the module. The design of the connector piece can be seen in figure 6.1. The thickness of the flat part of the connector pieces was chosen to be 5mm, so that air channels could be embedded in the design. This 5mm adds to the non-bending length of the module, making the total module 50mm in length. Protrusions on both side of the connector pieces embed within the endoscopic modules. Either within the chamber channels, or within the central cylinder that is used for guiding surgical instruments. This way the connector pieces can be aligned with the module during fabrication, giving a more consistent result. Alignment in rotation around the axis of the modules still has to be performed by hand, which can create slight differences in the expected and measured bending directions.

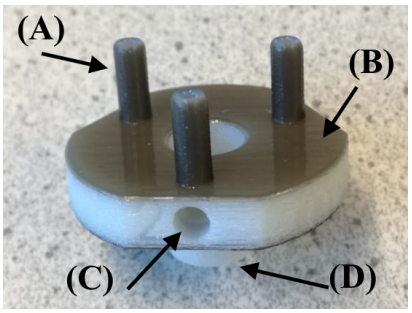

Figure 6.1: The 3D-printed connector piece, with (A) the connections to the pneumatic chambers, (B) the thin layer of a slightly poreous structure for the interface to the silicon rubber of the module, (C) one of the connections for the supply pressure, and (D) the connection to the central cylinder of another endoscopic module.

VeroWhite is used as the base material in the fabrication of the connector pieces. A thin layer of AgilusBlack (StrataSys, Ltd.) is used to created a slightly poreous structure at the interface that has to be glued to the silicone rubber of the module. Multiple tests were performed to find the right method and materials for connecting the connector pieces and the silicone rubber. An Object260 was used for printing the connector pieces.

Each new module is finished by adding a single connector piece, so that pneumatic tubing can easily be connected. The junction between module and connector piece was tested by applying a pressure to a single chamber and increasing this pressure in steps until the glue connection failed. The tested module could withstand at least 1.5 bar of pressure in each chamber and the first connection failed at 1.75 bar. The chambers of the module itself were still intact. After this test, it was decided to keep the operating pressure below 1 bar to prevent failure of the connections between the modules. Better connection methods could lead to safe operation at higher pressures, giving higher bending angles.

Using a maximum of 1 bar of supply pressure, the maximum operating range of the endoscopic module can be determined. For practical applications it might be desirable to be able to reach the same bending angle for all possible bending directions. The bending range of the endo-

scope will therefore be defined as the maximum amount of bending that can reached in all directions using 1 bar of pressure at most. Although higher bending angles can be reached in certain directions (in dual chamber actuation for example), these will not count for the bending range of the endoscope. The bending range of the soft robotic endoscope can be represented by a circle that fits entirely within the constant maximum pressure lines of figures 4.4 and 4.10. An example of this is shown in figure 6.2. The bending range of the endoscope gives a guaranteed amount of bending in all directions.

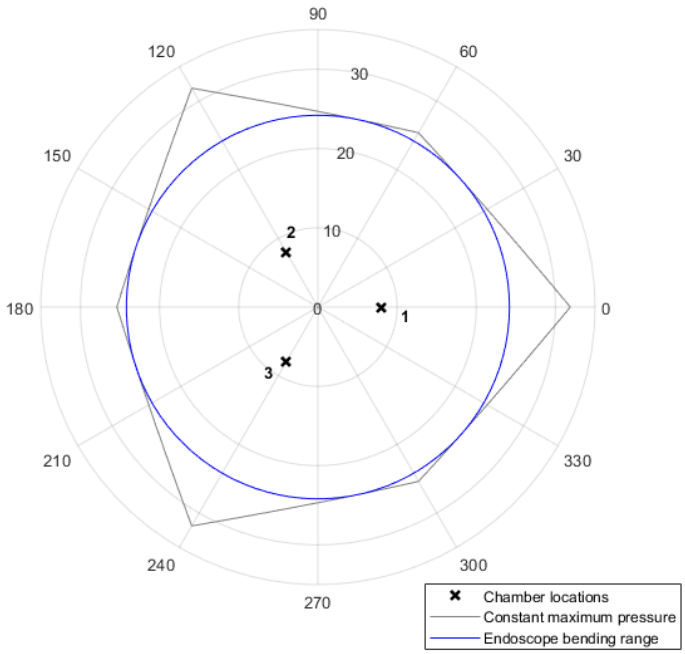

Figure 6.2: Drawing a circle that fits within the maximum reachable bending angles, based on a constant maximum pressure of 1 bar, reveals the bending range of the soft robotic endoscope.

6.2.2 Control system

Two pneumatic driver shields are added to the setup so that nine solenoid valves can be controlled independently. The additional driver shields are controlled via the same Arduino UNO via the unused digital outputs of the microcontroller. A total of three pressure regulators are used to control the whole endoscope. Each pressure regulator is used for a single module and connected to the input of three solenoid valves, as can be seen in the schematic drawing in figure 6.4. By activating the right solenoid valves, either one, two, or three chambers of a module can be actuated simultaneously. Because each module has a single pressure regulator, it is not possible to have separate chambers at different pressure levels within the same module in order to generate every desired bending direction. Using this setup, every module is therefore restricted to six bending directions only. The bending angles can be varied over the whole range. For use of the whole theoretical range of the 3-module endoscope, a total of nine pressure regulators are required. Chapter 7 will introduce a solution with which only a single pressure regulator is required for the whole endoscope, even though the whole theoretical range can be reached.

The software is updated so that nine solenoid valves can be controlled with the setup shown in figure 6.4. The actual hardware is shown in figure 6.3 and the updated UI can be seen in figure 6.5.

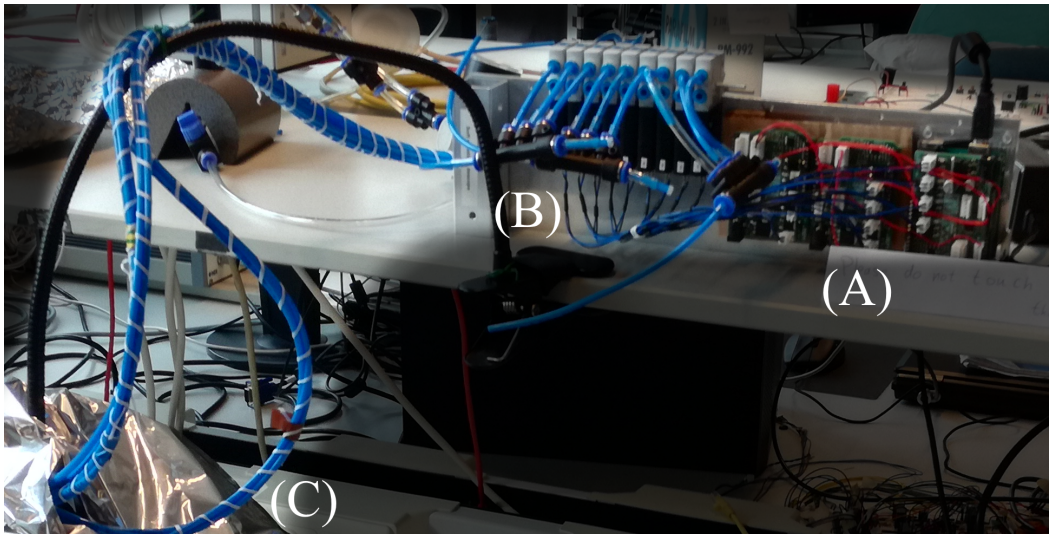

Figure 6.3: The setup for controlling the soft robotic endoscope, with (A) three pneumatic driver shields, in order to control nine solenoid valves and three pressure regulators, (B) nine solenoid valves, of which the connections depend on the experiment, and (C) the pressure tubes running towards the soft robotic endoscope (that is not shown).

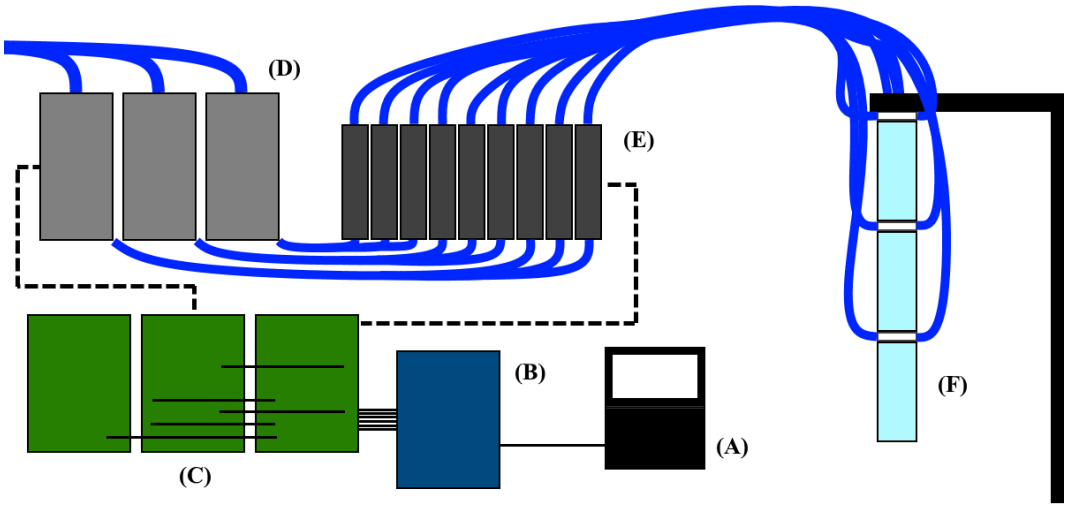

Figure 6.4: The setup for controlling the multi-module endoscope, with (A) a computer running the Matlab app, (B) an Arduino UNO that acts as the peripheral between software and hardware, (C) three pneumatic driver shields, (D) one pressure regulator per module of the endoscope, (E) one solenoid valve per chamber, and (F) the multi-module endoscope itself.

6.3 Validation method

The soft robotic endoscope should be able to follow the curvature of the environment during surgery. This means that it should be possible to control the configuration over the whole length of the endoscope. To validate that this is possible with the setup, several configurations will be used as setpoints. These setpoints will be used to calculate the theoretical configuration of the endoscope, of which a drawing will be made to scale. The bending of the endoscope will then be recorded using a camera and both pictures will be overlayed to compare.

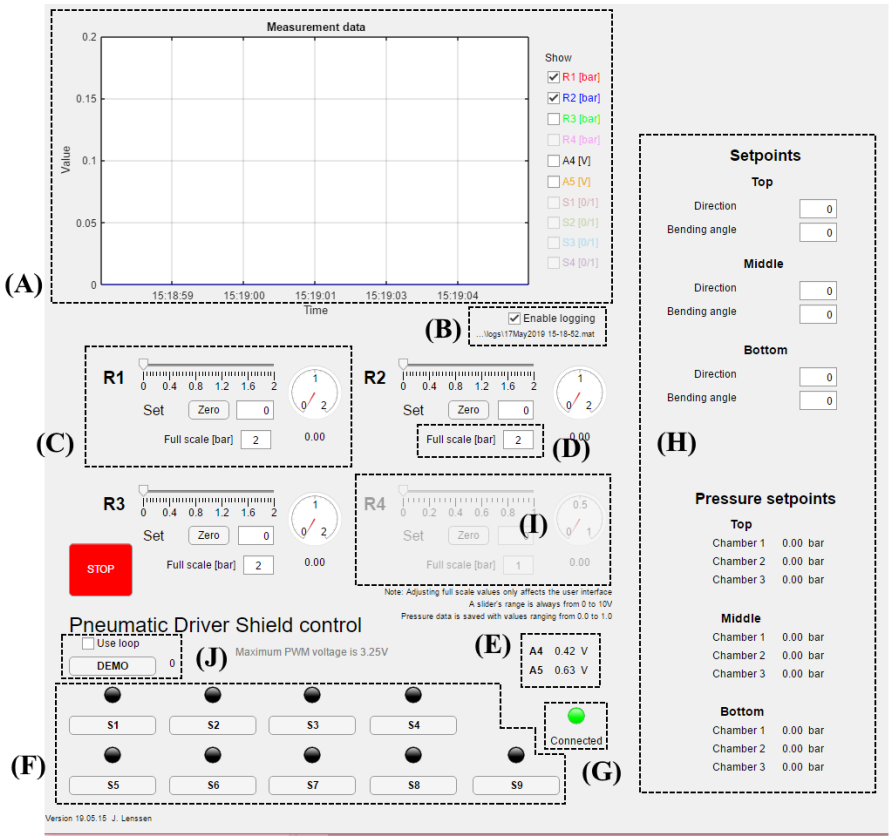

Figure 6.5: The UI for controlling the soft robotic endoscope with three pressure regulators and nine solenoid valves, including the inverse physical model that calculates required chamber pressures based on bending angle and direction setpoints. With (A) the plotted measured data for the selected inputs (feedback from regulator Ri, analog input Ai, or the state of solenoid valve Si), (B) the controls for saving the measured data in a log file, (C) the controls for, and feedback from, a single pressure regulator Ri, (D) the edit field for setting the full scale pressure of the pressure regulator that is used, (E) the measured values of the auxiliary analog inputs Ai, (F) the buttons for setting the state of the solenoid valves Si, (G) the indicator for showing whether or not an Arduino UNO has been connected, (H) the inputs for the bending angle and direction per module and the calculated pressure setpoints resulting from the physical model, (I) the grayed out pressure regulator 4, because the setup only uses three pressure regulators in total and the digital ouput pins used by regulator 4 have been routed to the control inputs of solenoid valves, and (J) the button for activating the demo routine that will load a series of setpoints which will be applied in order.

Because the endoscope with only a single pressure regulator per module can only bend in six directions, configurations will be selected within a place. Three-dimensional configurations will be tested in chapter 7, when the whole actuation space is available.

The configurations that will be tested are described in table 6.1. The bending angles are determined by the physical model by applying 0.97 bar per chamber. This is the actual pressure that is applied when the command for 1 bar is given, due to a slight deviation in the output of the pneumatic driver shield. A bending direction of 0° means that only chamber 1 is activated, while 180° means that both chamber 2 and 3 are activated. The shapes are created by commanding 1 bar (so that 0.97 bar is applied) and activating the right chambers.

Pictures of the endoscope are captured using a digital camera that is calibrated using the Matlab camera calibrator to remove distortions. Distances per pixel are calibrated using a checkboard pattern in the plane of the endoscope. The drawing of the predicted configuration of the endoscope is made by calculating the expected bending angle per module based on the pres-

Shape		Top	Middle	Bottom
'S'	*Angle*	30.5°	24.45°	30.5°
	Direction	180°	0°	180°
'C'	*Angle*	30.5°	30.5°	30.5°
	Direction	180°	180°	180°
'J'	*Angle*	0°	0°	30.5°
	Direction	0°	0°	180°

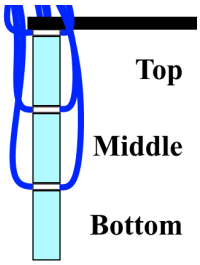

Table 6.1: The three validation shapes and the corresponding bending angles and directions per module

sures that were applied during the experiment. These bending angles correspond to the angles mentioned in table 6.1. The drawing contains the non-bending parts of the modules as well, so that the theoretical configuration of the whole length of the endoscope will be drawn.

6.4 Results and discussion

The three shapes from table 6.1 were used as setpoints and the bending of the endoscope was captured in figures 6.6a, 6.6b and 6.6c. The expected shapes of the endoscope based on the physical model were overlayed. The +'s in the shape show the transitions between bending and non-bending parts of the modules and the transitions between modules. It is assumed that only the part of the module containing the pneumatic chambers elongates. The initial length of this part is 3cm, compared to the 5cm of a single module with connector piece.

It is directly clear that the top module bends less than the bottom module with the same amount of pressure. It is expected that this is due to the loading of the module, both by the pneumatic tubes and by the weight of the rest of the endoscope. It can also clearly be seen that the top and middle module elongate due to the added weight of the lower modules (especially in figure 6.6c). Because the physical model only works for the unloaded case (although it can be extended when the forces are known exactly (Fraś et al., 2014)), the amount of bending reached in practice differs from theory. The bottom module, that is not loaded, shows bending as expected.

The difference between expected bending and bending in practice means that compensation for the external forces on the endoscope is necessary when position control is desired. Knowing what the differences are between expected angles (the setpoints) and the actual bending makes it possible to apply control for compensation. This should of course be done within the limits of the hardware, which has a maximum allowable input pressure of 1 bar. Despite loading due to gravity and the external tubes, it should be possible to reach any desired shape that lies in the capabilities of the hardware when position feedback is applied. The precision with which this can be done depends on the accuracy of the feedback and the pressure regulators.

It was already determined that the modules could not reach the required amount of bending in the unloaded case. With external loading, the bending performance becomes worse as the force that bends the module has to compensate for the external forces as well. In order to ensure a minimum amount of bending, the maximum external load should be determined and the force of the endoscopic modules should be made large enough to compensate for the right amount of bending. An increase of force can be achieved by applying a chamber pressure of more than 1 bar. While this is not allowed in the current design, the reasons for this are linked to the method of fabrication. Tests with higher pressures showed that the glue connecting the module and the connector pieces failed. The design of the module itself is highly likely to survive significantly higher pressures, because the strain in the material of the module is relatively low compared to the strain seen in modules with outer sheath (or with no sheath, as in figure 2.3). A better fabrication method could therefore allow higher pressures, which in turn would give larger bending angles. It should be noted that higher actuation pressures might pose a

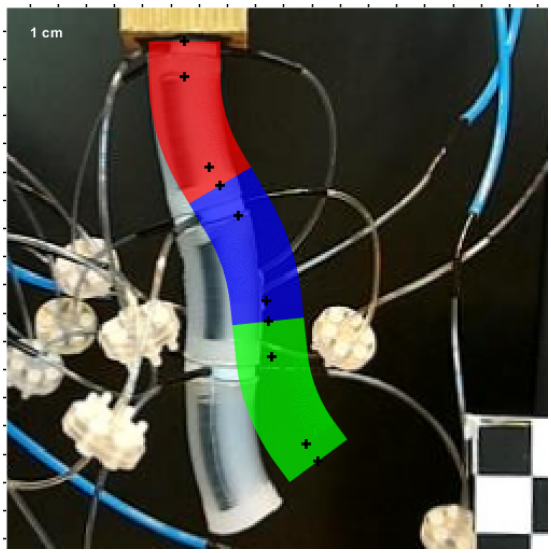

(a) The 'S' shape

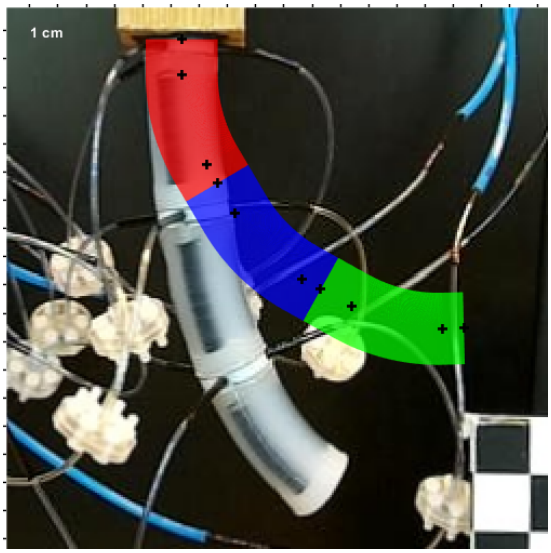

(b) The 'C' shape

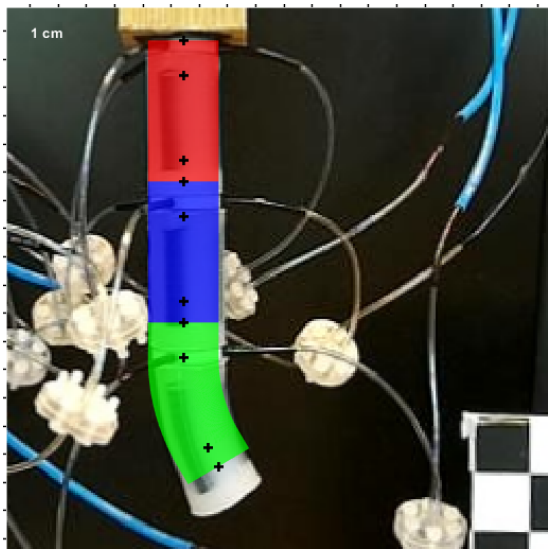

(c) The 'J' shape

Figure 6.6: Results of the two-dimensional validation of the multi-module endoscope

larger risk for patient safety, because the forces become higher and failure of the modules might lead to more damage.

6.5 Conclusion

A multi-module endoscope was made from three endoscopic modules and this endoscope was steered using feedforward control based on the physical model of the modules. Steering was only possible in six bending directions because only a single pressure regulator per module was available. Although the concept of steering the multi-module endoscope proved promising, the bending behaviour of the setup was significantly disturbed by external forces due to gravity and due to the required pneumatic tubing. It is clear that feedback is required for accurate position control. The goals set in the endoscope requirements were not met. For achieving these goals, the usable chamber pressures should be made higher by improving the fabrication methods. The endoscope requires more force in order to compensate for external loads and to be able to bend further.

7 Scalability

Scalability of the soft robotic endoscope is an important aspect when NOTES applications are considered, but has not been achieved in MR-compatible robotics, despite the large number of studies on the design of soft robotics (Laschi et al., 2016). A soft robotic endoscope that is scalable can be made suitable for surgical intervention in NOTES further away from the point of entry. NOTES requires the endoscope to be long in order to be able to reach the desired target. The current designs of robotic endoscopes are either not suitable for use under MR guidance, or are not to scale. This chapter therefore aims to alter the design of the endoscopic module to achieve scalability.

The most important factors limiting the scalability of the endoscope are the dimensional requirements for sufficient actuation force, the stiff pneumatic tubing and MR-compatibility that prohibits the use of internal electronics. Each module requires its own set of pressure tubes that supply the actuation pressures for the different chambers. While the drawbacks of decreasing the module dimensions can be partly solved by using higher actuation pressures, the amount of tubes that have to run through the endoscope limit downscaling beyond a certain point. In order to solve the scaling issue, a new actuation method using micropneumatic valves (airlocks) will be developed and tested. Steps will be taken to build an endoscope that includes pneumatic logic that can take over the role of electronics in other, similar, modular robotic snake-like actuators such as V-SPA (Robertson and Paik, 2017).

The result of this chapter will be a modular soft robotic endoscope that includes pneumatic valves in order to demonstrate the actuation principles of the modular endoscope. The performance of the endscope will be compared to theorical results again. Using only pneumatic valves, the size of the pressure tubes can already be decreased and only a single pressure regulator is required for controlling a 3-module endoscope.

7.1 Analysis and theory

Many aspects of the design influence the scalability of the endoscope. The most important factor, however, is the set of pressure tubes and the routing through the endoscope.

7.1.1 Pneumatics for the soft robotic endoscope

For every pneumatic chamber to have its own connection to a pressure regulator, in order to be able to set all pressures independently for a continuous actuation range, the number of tubes through the endoscope has be equal to the total number of chambers. This is equal to three times the number of modules and for the 3-module endoscope, this means nine pressure tubes. Every pressure tube running through the endoscope will use a certain area, or footprint, that is no longer available for other components such as the pneumatic chambers. If the footprint becomes too large, it might determine the minimum diameter of the endoscope, which limits the scalability.

Using the smallest diameter tube in the lab, with an inner diameter of 1mm and an outer diameter of 2mm, and neglecting the fact that circular tubes cannot be packed with 100% efficiency, this would already require a footprint of $28mm^2$. This is more than half the area of the empty central cylinder in the modules ($(4mm)^2\pi = 50.3mm^2$). A six module endoscope would already require more space than the central cylinder provides and would suffer from the stiffness the extra tubes provide. Next to this, the smallest tubes also provide the least amount of flow. Although the endoscope is not required to react quickly, the delays introduced due to this restriction might cause instability in the control of the chamber pressures. This means that

the controllers in the pressure regulators have to compensate for the effects of the pneumatic tubes.

A good example of a modular and scalable pneumatic robot is V-SPA (Robertson and Paik, 2017), which uses a single supply of vacuum and local solenoid valves for actuation. The solenoid valves can be activated using addressable electronics. This way, the number of tubes or electrical wires in this design does not depend on the number of modules. The use of electrical components makes this design unsuitable for MR applications, however. The idea of a single supply that can be used by all modules independently is the core strength of this design and can be used in the MR-compatible endoscope as well. This can be done by replacing the electronic components by pneumatic systems that function similarly.

7.1.2 Pneumatically activated airlocks

A novel method of actuating the pneumatic chambers is by using pneumatic valves, or airlocks because of their function as a lock, that can connect or disconnect the chambers from a main pressure supply. When the lock is opened, the chamber pressure is equalized to the supply pressure, and when the lock is closed, the chamber pressure and supply pressure can differ. This way only a single pressure regulator is required for all pneumatic chambers in the endoscope, because closed chambers can stay pressurized while other chambers are brought to a different pressure level. The airlocks are similar in function to the solenoid valves used in V-SPA. The main problem is that the airlocks also have to be activated using MR compatible methods.

The airlock can be activated using another positive pressure which opens or closes the path for the supply pressure. Similar to the pressure in the pneumatic chambers, the control pressure can exist without flow. Supplying this air pressure can be done via the smallest tubes, in contrast to the case of supplying the chambers pressure. This is because the control reservoir can be made small compared to the pneumatic chamber volume, giving a low time constant. Care should still be taken to prevent overshoot at the control input of the airlocks, but this overshoot will not increase the chamber pressure and can therefore be tolerated as long as the airlocks can withstand the pressure. If the system starts oscillating, which might open or close the airlock unexpectedly, undesired behaviour might still occur.

Using small tubes for activation of the valves decreases the amount of space the tubing requires. This in turn decreases the influence of the tubing on the behaviour of the endoscope. The influence can be lowered even more when another equivalent of electronics is used, namely logic gates. By combining the valves that can be pneumatically activated, it is possible the create logic gates using pneumatics. Examples of this are shown by Henning (Henning, 2007).

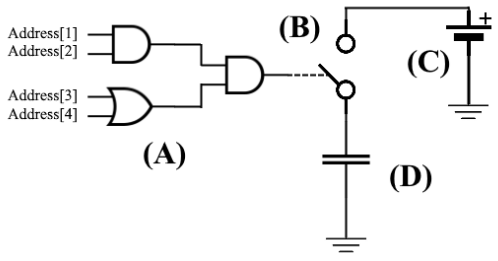

Figure 7.1: The idea of pneumatic logic gates expressed in electrical schematic symbols, with (A) the logic gates combining to form a single actuation single from (in this example) four address lines, (B) the switch that can be opened or closed by the actuation signal from the logic circuit, (C) the (variable) supply, and (D) the storage element that represents the pneumatic chamber. Please note that the influence of the pneumatic lines is not modelled here.

The electrical equivalent of this pneumatic system is a circuit with MOSFETs and actual switches, fed from a single supply, that are activated using logic signals that can be altered using logic gates. A schematic representation of this can be seen in figure 7.1. The airlock is analogous to the switches, while the logic gates can be constructed using technology that is similar in behaviour to the MOSFETs. Chamber actuation will be done in order by addressing the chambers in sequence. The sequence is demonstrated in figure 7.2. The generation of the logic signals can be done by solenoid valves that translate the signals from the electrical domain to the pneumatic domain. Without the integrated pneumatic logic, every airlock requires its own solenoid valve and signal pressure line. By using the integrated logic, the number of signal pressure lines for the whole endoscope becomes significantly smaller.

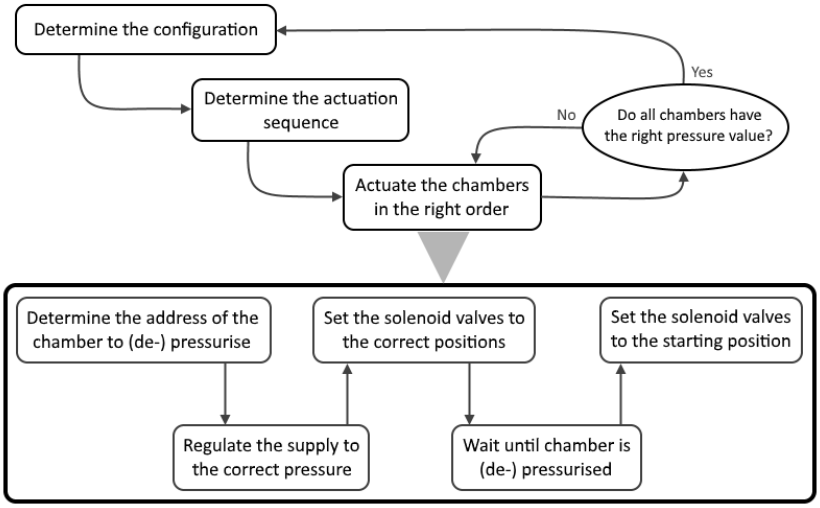

Figure 7.2: The control sequence for addressing all individual chambers in the soft robotic endoscope using addressable airlocks

Using this sequential approach and the integrated logic elements, the number of solenoid valves and small diameter high pressures lines required for a certain total number of chambers in the whole endoscope, n, is equal to $log_2(n-1)$ rounded to the first higher integer. This means that binary addressing is used and that one of the combinations of bits is required to select none of the chambers (the 'starting position'). Connecting five 3-chamber modules, for example, gives a total of 15 chambers. This requires 16 different addresses, or four bits and signal pressure lines. The number of pneumatic tubes scales with $log_2(n)$ using pneumatic logic, compared to n when a signal pressure line per chamber is used.

7.2 Design

Based on the method of using airlocks for addressing the pneumatic chambers, a concept design for the complete soft robotic endoscope was drawn in figure 7.3.

7.2.1 Design of the airlock

The function of the airlock is to open or close the channel between the main supply line and a chamber. A design was made and a prototype was 3D-printed using the Object260 and the material VeroClear. The airlock consists of two pieces that clamp on both sides of a silicone rubber membrane of 0.5mm using six nylon M3 bolts and nuts. A schematic view of the airlock can be seen in figures 7.4 and 7.5. The stacking of layers in the design was made to be easy for printing and assembly.

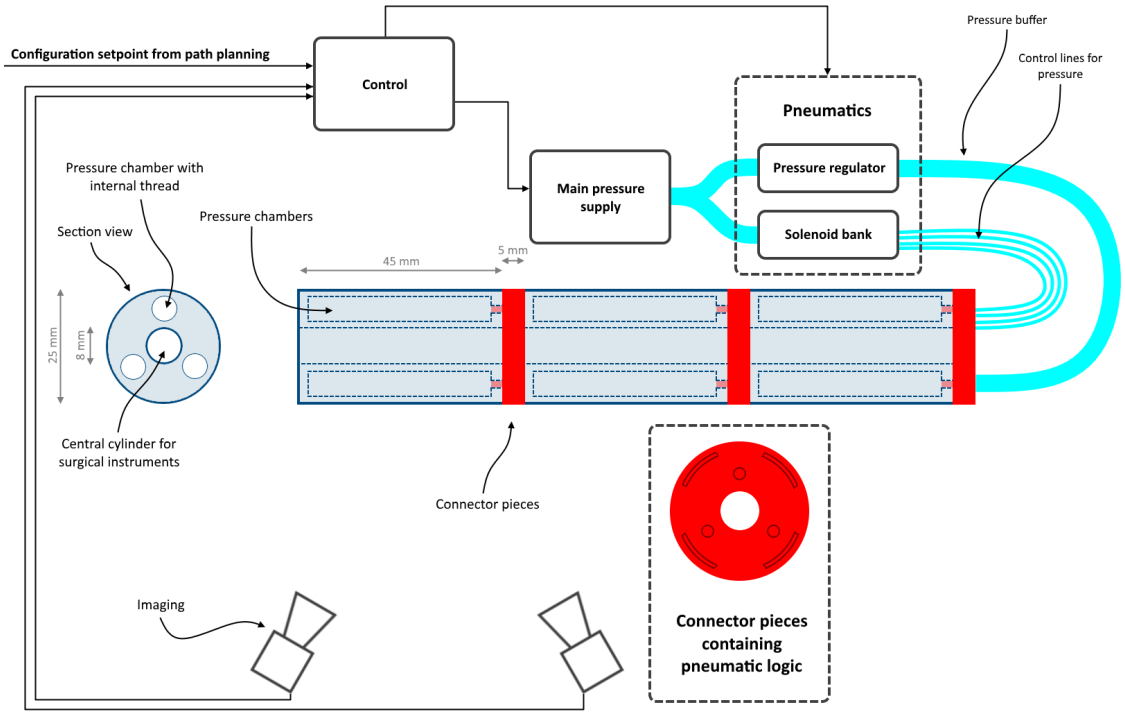

Figure 7.3: The concept drawing for the complete soft robotic endoscope, containing the dimensions of the prototype and the methods using pneumatic logic and airlocks. Feedback in the form of imaging is shown as well, even though this was not implemented in this project.

Closing the airlock is achieved by pressing a flexible membrane against the input and output channels of the airlock using a signal pressure. The airlock is opened by removing the signal pressure, so that the membrane bends back and the channel between input and output becomes clear. Using a positive pressure for closing the airlock means that the closing action is not dependent on the spring force of the membrane. This aids in downscaling the design, because the required force comes from an external source and not from the material itself. It also means that very low input supply pressures are enough to let the membrane bend back to open the channel when the control reservoir is at ambient pressure. Using a positive pressure makes the system more safe as well, because removing the control pressure in an emergency will open all airlocks so that the endoscope becomes passive (without force) and flexible.

The assembled airlock can be seen in figure 7.6. This prototype is at a larger scale and serves as a proof of concept for the later integration in the endoscope. Eventually, the airlocks have to be integrated into the connector pieces between the modules, as could be seen in figure 7.3, in order for the concept to aid in downscaling the endoscope. While a design was made for such a connector piece based on the larger scale airlock, fabrication issues in the 3D-printing of fine details of the design lead to leaks. This is why only a proof of concept was tested using the larger scale airlocks outside of the chambers, connected within the supply lines of the chambers. Figures of the original design can be found in appendix C.

In order to check the working principle of the airlock, several airlocks will be characterized to determine the control pressure required for keeping the lock closed at different supply pressures.

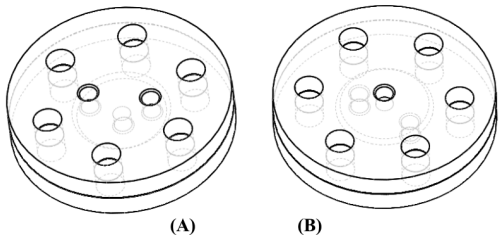

Figure 7.4: Schematic view of the airlock, with (A) the supply input and chamber connection side, and (B) the signal pressure side. The six holes around the circumference are for placing the bolds and nuts for clamping the sandwich together. The diameter of the disc is 25mm, its thickness is 5.1mm (including the 0.1mm thick membrane, which was eventually chosen to be 0.5mm) and the holes for the pressure connections have a diameter of 2mm.

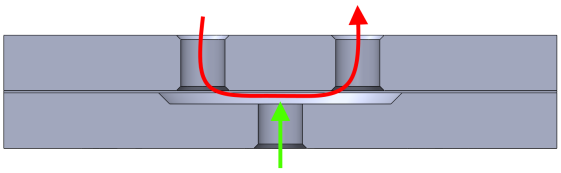

Figure 7.5: Cross-section view of the airlock, showing both 3D-printed pieces and the membrane in the middle. The red (top) arrow indicates the flow between the pressure supply and the pneumatic chamber and the green (bottom) arrow shows where the signal pressure is applied to close the valve.

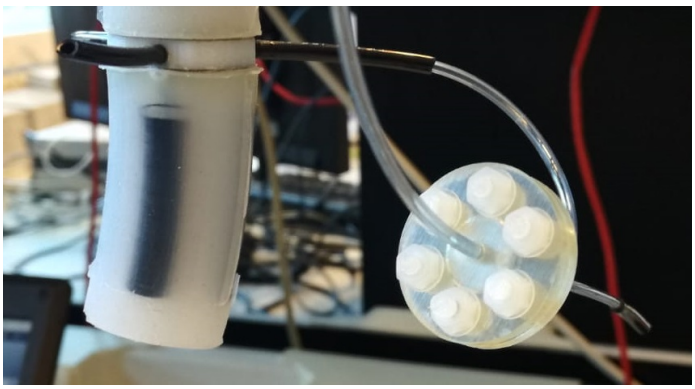

Figure 7.6: The prototype airlock keeping a chamber pressurized. The supply input of the airlock was disconnected after the airlock was closed.

7.2.2 Design of the control system

Hardware

The endoscope and setup from chapter 6 are altered to include the prototype airlocks. Nine airlocks are fabricated and connected in between the main pressure supply and the chambers. The main pressure is supplied by a single pressure regulator that is controlled via the pneumatic driver shield and software. A constant control pressure of 1.3 bar is fed to all nine solenoid valves, which are connected to the control signal inputs of the locks. Switching a solenoid valve therefore switches a single airlock. Opening a solenoid valve to allow 1.3 bar on the airlock closes the lock. Closing the solenoid valve supplies ambient pressure to the airlock, opening it. A schematic representation of this setup can be seen in figure 7.7.

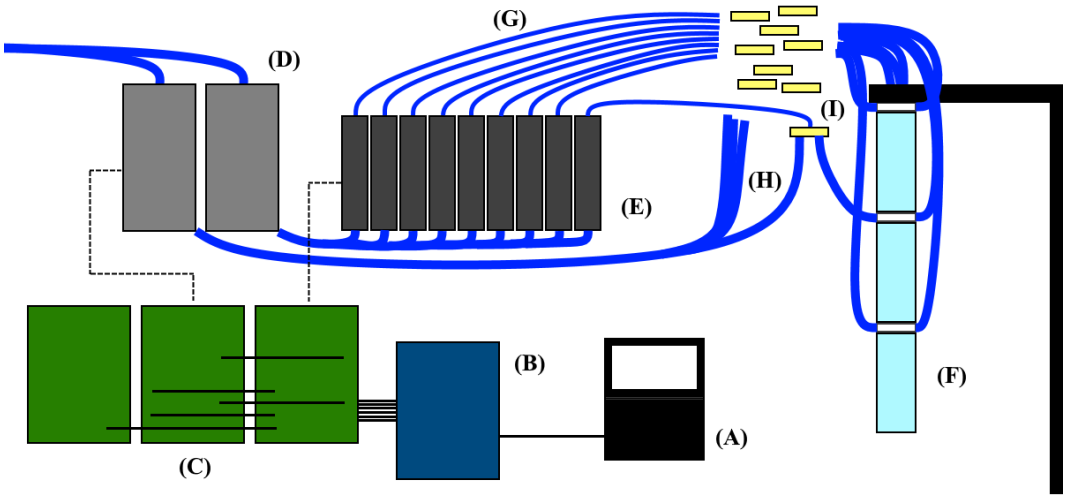

Figure 7.7: The setup with the soft robotic endoscope connected via airlocks, with (A) a computer running the Matlab app, (B) an Arduino UNO that acts as the peripheral between software and hardware, (C) three pneumatic driver shields, (D) one pressure regulator for supplying signal pressure and one pressure regulator as the main supply of the chambers, (E) one solenoid valve connected to signal pressure per airlock, (F) the multi-module endoscope itself, (G) the signal pressure lines to the airlocks, (H) the main pressure supply to the input of the airlocks, and (I) one airlock per pneumatic chamber.

Software

A software routine implementing the control sequence explained in figure 7.2 is written and added to the Matlab app. The actuation sequence was chosen to be a sequence of stepping through all chambers in order. The required pressure per chamber is applied directly, which means that the endoscope will react almost instantly and that the configuration is reached in a single cylce of addressing all chambers. The software will continue cycling through the chambers indefinitely, which means that every chamber will be repressurized once every cycle. Configuration changes can be made at any time, but the addressing cycle will not reset. This means that it might take a full cycle before the new configuration is reached.

The configuration is determined by setting the bending angle and bending direction per chamber. The responsible UI elements were shown in figure 6.5. The physical model is used for calculating the required chamber pressure. In the final application of the endoscope, it is assumed that the configuration of the endoscope will be the result of path planning. This also means that care has to be taken to pressurize the chambers in the right order, because the whole length of the endoscope will have to follow the curvature of the environment. Configuration changes that are too big might lead to collosions or excessive force, which can lead to painful surgery. This also means that it might be necesssary to wait for multiple cycles before the new configuration is reached, as smaller steps per chamber might be necessary to avoid collosions. An example of this is shown in figure 7.8.

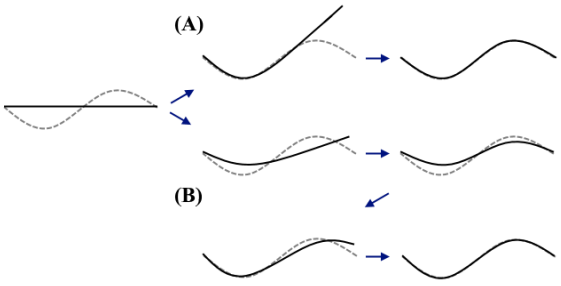

Figure 7.8: Two methods of reaching a final configuration with two modules using sequential steps, with (A) the fastest approach and (B) by using intermediate steps to prevent excessive swing of the last module.

7.3 Characterization and performance assessment

7.3.1 Method of characterization of the airlocks

In order to check the working principle of the airlocks, the blocking behaviour of the airlock will be characterized. This will be done by applying different input pressures and signal pressures and measuring the output pressure. The 'demo' routine of the Matlab app is used for this measurement to control the input pressure and the signal pressure. An oscilloscope is connected to the analog input signals of the input pressure, the signal pressure, and a pressure sensor (40PC015G, Honeywell) that measures the output pressure of the airlock.

A sequence is loaded in the routine that ramps down the signal pressure starting from 1.3 bar in steps of 0.05 bar. This ramp is repeated for different values of input pressures starting from 0.1 bar which is increased in steps of 0.1 bar up until 1 bar. Every ramp of signal pressure is logged, together with the other measured signals. The pressures at which the output pressure increases suddenly is written down. This is the point where the airlocks opens because the control pressure has become too low.

Because the airlock design is symmetrical, that is, the input and output pressure channels are equal, the behaviour of the airlock is also expected to be symmetrical. This means that it does not matter whether the input pressure is higher than the output pressure, or the output pressure is higher than the input pressure. This is why only an increase in input pressure is measured and the output pressure is reset to 0 bar every ramp of signal pressure.

7.3.2 Method of assessing the performance of the endoscope with airlocks

The performance of the endoscope with airlocks will be assessed by commanding different shapes using the same principles that were used in chapter 6. Because the whole actuation range should now be reachable, the shapes of the endoscope will be viewed from two different directions (90° apart), so that the 3D bending configuration will become clear. The shapes that will be commanded are listed in table 7.1.

Shape		**Top**	**Middle**	**Bottom**
'S'	*Angle*	24.36°	24.36°	24.45°
	Direction	30°	90°	0°
'C'	*Angle*	24.36°	24.36°	24.36°
	Direction	30°	30°	30°
'J'	*Angle*	0°	0°	24.36°
	Direction	0°	0°	30°

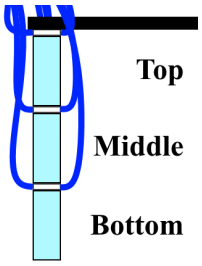

Table 7.1: The three validation shapes and the corresponding bending angles and directions per module for three-dimensional validation

Because the tip of the endoscope is the part that will have to point to the surgical target, the range of the tip will be validated as well. This is done by projecting multiple targets on a bowl (half sphere) below the endoscope and having the endoscope 'look' at these targets. A small camera will be placed inside the endoscope and connected to a laptop for direct viewing. For a completely steerable endoscope, it should be possible to steer the camera so that the targets move exactly to the center of the view. The distance between the target and center of the camera view is a measure for the performance of the endoscope. A smaller distance means a more accurate endoscope. The endoscope will be controlled manually and only the bottom module will be actuated to simulate target finding in a clinical setting. At the start of the experiment, the tip of the endoscope will be placed in the middle of the (half) sphere and is pointed straight down towards the first target. A couple of targets surround this central target. The closest two targets are on a line that lies in the direction of 30° in endoscope direction coordinates. A bending angle of 18° is necessary to point at these targets.

7.4 Results and discussion

7.4.1 Airlocks

Three airlocks have been characterized in accordance with the methods described. The results of the characterization can be seen in figure 7.9. For two of the airlocks it is clear that the control pressure should be higher than the supply pressure, while the third airlock opens when the control pressure is at most 0.1 bar below the supply pressure. The characterization results show the points at which the supply pressure can reach the output of the airlock, meaning that the lock is opened. To ensure that the lock stays closed when it should, the control pressure should stay far enough above the supply pressure. This is why the setup of the multi-module endoscope will use a control pressure of 1.3 bar, which is at least 0.3 bar above the mximum allowable supply pressure.

What has been neglected in this experiment is that the supply pressure and the output pressure can both be high at the moment the airlock should be closed. In this case, the control

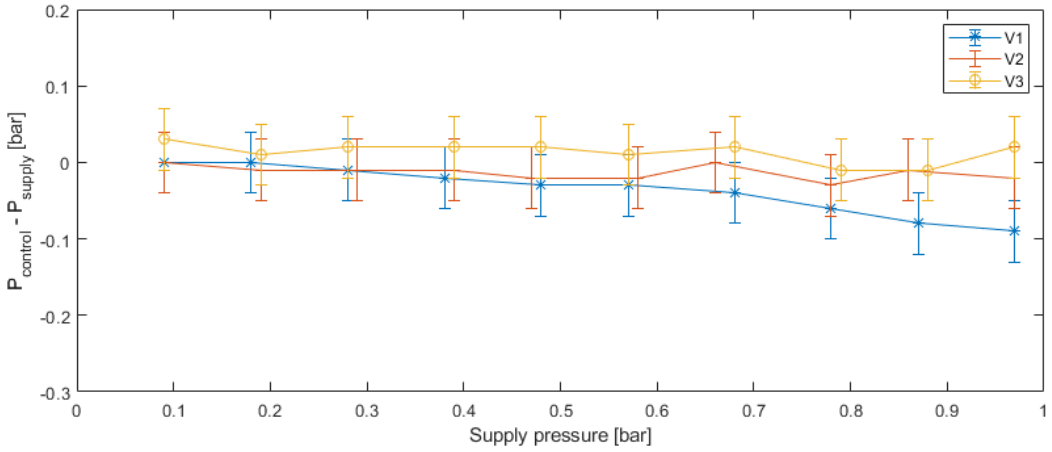

Figure 7.9: The required difference in control pressure compared to supply pressure for three different airlocks measured with input pressures from 0 bar to 1 bar. A positive value means that the control pressure had to be higher than the input pressure to keep the lock closed.

pressure has to overcome the force from input and output pressure combined. It is expected that the difference between supply pressure and control pressure has to be higher in this case. This is why the control pressure margin was chosen to be more than ten times the maximum measured (positive) difference between control pressure and supply pressure in figure 7.9.

Next to activation by air pressure, it would also have been possible to use a different method. Another way of actuating the valve is by using thin wires that run through the endoscope, but this would require compensation for the wire length when the endoscope bends or elongates. If not properly compensated, the force from the endoscope might open or close an airlock, leading to undesired behaviour. The method with wires is similar to what is used in other types of continuum robots for actuation, such as the Medrobotics' Flex (Johnson et al., 2013). Using wires would significantly decrease the space required for activating the airlocks, as the wires may be much thinner than the pressure tubes.

7.4.2 Endoscope performance

The shapes from table 7.1 were commanded using the UI running the routine for addressing all chambers in sequence. The resulting shapes can be seen in figure 7.10. It is clear that the endoscope can be positioned in three dimensions, even though only a single pressure regulator was used as a supply. This means that the airlocks can be used for controlling the multi-module endoscope and that the amount of hardware is significantly decreased by doing so.

The results of chapter 6 already showed that the amount of bending of the multi-module endoscope is heavily influenced by external factors. This is also true for validation in three dimensions. This why the three dimensional validation was performed using the target finding exercise as well. Figure 7.11 shows different spots on the surface of the half sphere that were targeted using manual control of the bottom module of the endoscope. The same addressing scheme was used and it was possible to steer the endoscope towards the two targets neighbouring the central target. This means that the endoscope could be controlled to reach two targets in the direction of 30° and 210° respectively, width a bending angle of 18°. While the angle of 18° lies within the expected bending range, the directions that were reached show that the airlocks make steering the bending direction with sequential addressing possible. This means that scalability was improved.

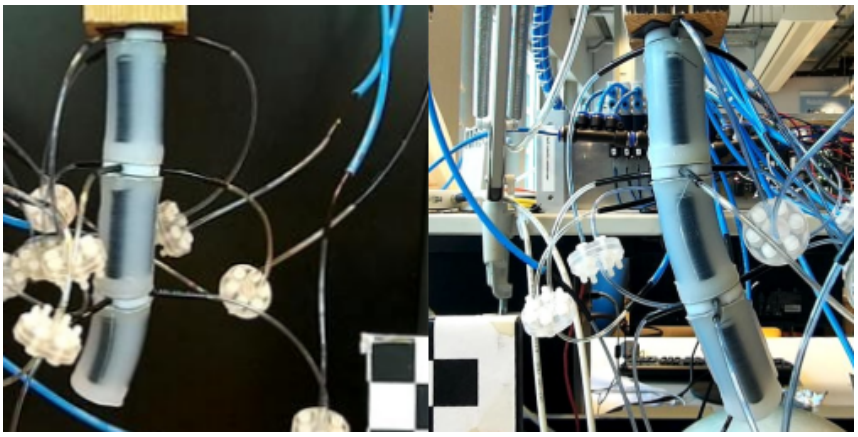

(a) The three-dimensional 'S' shape

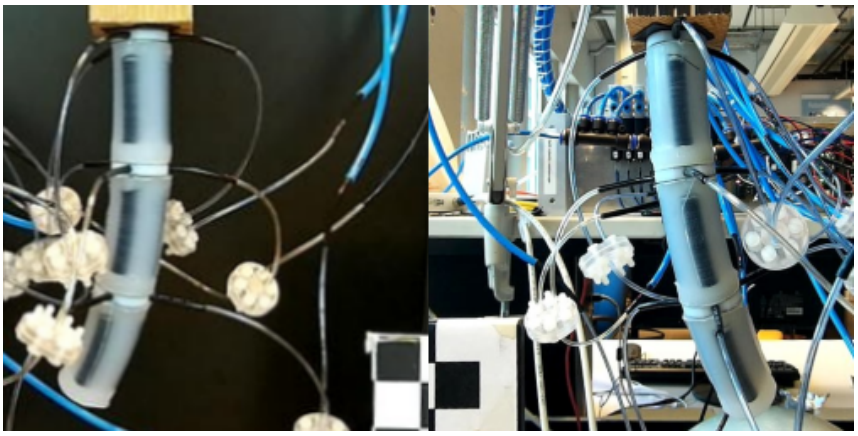

(b) The three-dimensional 'C' shape

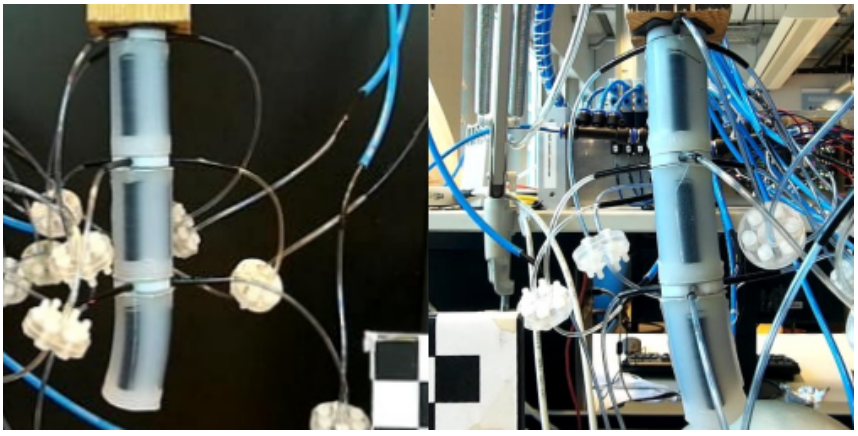

(c) The three-dimensional 'J' shape

Figure 7.10: Results of the three-dimensional validation of the multi-module endoscope with the use of airlocks

While the three-dimensional validation shows the working principle of the airlocks, the resulting shapes are not clear. A comparison to theory, similar to the comparisons performed in figures 6.6a, 6.6b, and 6.6c, would be beneficial. Because the shapes are defined in three dimensions, a three-dimensional model of the shape of the endoscope based on the physical model is required. For the comparison, this three-dimensional model must be projected on the two viewing planes used in figure 7.10. From the results of chapter 6 it should already be clear that large discrepancies in the theoretical and measured shapes are expected.

Although not visible in the figures, the endoscope was not completely stationary during the control sequence of the validation. This was caused by small leakages within the connections to the modules and the airlocks. A pressurized chamber should stay pressurized in order for the bending angle and direction to stay constant, as different chamber pressures result in different behaviour. All chambers were brought back to the required pressure during every loop of the addressing sequence, and this expressed itself in jumps of a couple of degrees for the chambers that leaked the most. A better setup is required to determine the cause of the leaking, although first tests indicated that the tansitions between two different tube diameters were not completely leak proof. Out of the nine airocks, only three have been characterized in figure 7.9, which means that leakage could also be caused by manufacturing errors in the airlocks. During surgery, and especially when precision is required, this leakage cannot be tolerated, as it lowers the accuracy in positioning.

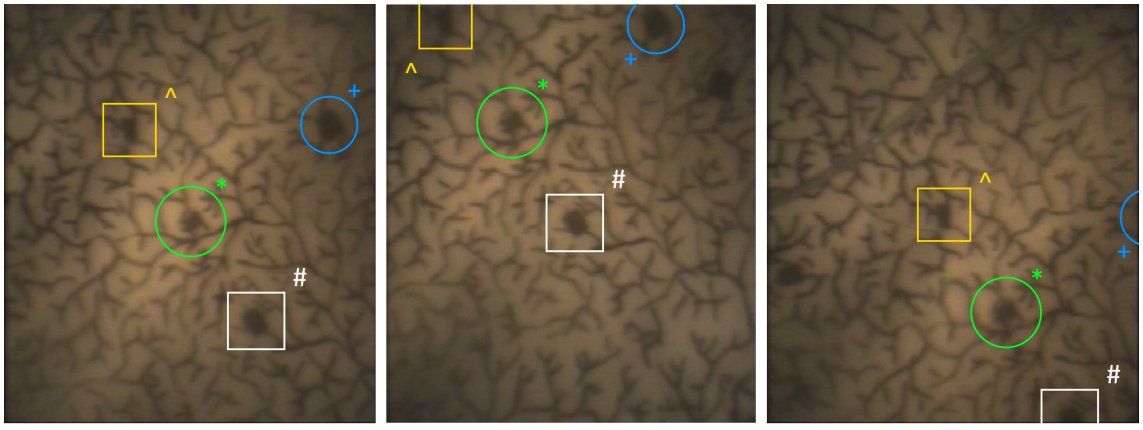

Figure 7.11: Stills from the target finding exercise. The camera was initially placed as in frame (A). It was then moved from frame (A) to frame (B) and from frame (B) to frame (C) using the UI. Required bending angles and directions were manually entered for the bottom module and small steps were taken to reach the targets, with the goal of positioning the targets in the center of the screen. The upper two modules were left unpressurized. All targets are marked in each still.

7.5 Conclusion

A multi-module endoscope using micropneumatic airlocks was realized and tests showed that it was possible to control the endoscope in the whole actuation range permitted by the maximum input pressure limitations. The airlocks proved functional and the required control pressure was determined. It was found that the control pressure should be at least 0.3 bar higher than the highest expected chamber pressure in order to compensate for manufacturing differences.

It was hypothesized that integrating the airlocks in the connector pieces, together with micropneumatic logic gates, can aid in significantly reducing the hardware that is necessary for controlling the soft robotic endoscope. With the prototype airlocks it was already demonstrated

that only a single pressure regulator is required for controlling an endoscope with a total of nine pneumatic chambers. Because the setup contained leaks and the endoscope suffered from relatively large external influences, more measurements are required to determine to what extent and with what accuracy the scalable soft robotic endoscope can be steered.

8 Discussion and recommendations

8.1 The endoscopic module

For the realization of an MR-compatible soft robotic endoscope for MIS and NOTES, it turned out that the 3-chamber inner sheath STIFF-FLOP like module was the most suitable. The design of MOLLUSC was therefore altered to contain 3 pneumatic chambers with inner sheathing. Only the necessary changes were made, which means that in terms of dimensions, the new module and MOLLUSC are comparable. The new design might therefore not be optimal in terms of the amount of bending that is possible with a module with these dimensions. The maximum bending angle at 1 bar of the module was found to be around 25° for single chamber actuation. It is expected that this can be increased significantly with the same type of module by finding the optimal design parameters.

Compared to MOLLUSC, the bending angle of the new module is much smaller. The reason for this is the difference in chamber diameter at higher pressures, due to the expansion of the chambers in MOLLUSC. While the new module has improved linearity and controllability, the maximum bending angle of the module does not meet the requirement of at least 40° of bending. It would therefore be beneficial to work towards increasing the maximum bending angle of the 3-chamber inner sheath module. This could be done by increasing the chamber size, decreasing the stiffness of the material that is used or increasing the maximum pressure the module can safely handle.

While there are possible solutions for increasing the bending angle of the modules, the reason for this lower than expected bending is not entirely clear. The finite element simulations of the modules gave bending angles that were more than three times as high as the measured angles. The expected cause of the differences between experiments and simulations is the difference in chamber dimensions and shapes. Experiments should be performed to better validate the simulation results and check whether the difference in cross sectional area can completely explain the differences in the results.

Although the volumetric design of the chambers was not changed from the basic circular design, it could be beneficial to look into the other volumetric designs in order to design a smaller module with more space for pressure tubes. To validate the results of the finite element models with different volumetric designs, modules have to fabricated and the bending angles have to be validated.

8.2 Steerability

Steering of the endoscopic modules was realized using feedforward control with a physical model based on characterization. While this method works in the unloaded case, the multi-module endoscope showed that external influences impact the bending behaviour of the modules and that feedforward control is not accurate enough. This is why it would be beneficial to do research in the direction of control with feedback. This can be done using MR-compatible sensors, or by making use of imaging techniques that can recognize and extract the configuration of the endoscope. Any disturbance in the positioning can then be corrected to ensure safe and desired behaviour. Next to the forces due to the weight of the endoscope, the added stiffness of the surgical instruments is expected to introduce large disturbances as well. Experiments must therefore be performed to measure the influence of these instruments.

The physical model of the module was improved compared to the model from literature, but also requires more research. Although it is expected that the decrease in second moment of area of the module due to elongation plays a significant role in the increased bending, this was not demonstrated. For a better understanding of the behaviour of the module at higher pressures,

it is necessary to look at the exact cause of the increase in bending. Although the elongation is expected (which could be linked to a decrease in second moment of area), the elongation was not measured and a conclusion can therefore not be drawn.

For the control of the module it was hypothesized that the length of the pneumatic tubes can have a large influence and can even lead to an unstable system. The tubes were therefore kept short, although this is not in accordance with the final application were the electrical hardware has to be placed far away from the endoscope. Models should therefore be created to gain insight in the effects of tubing and experiments should be performed to assess whether or not a sufficiently large and fast input signal can lead to an unstable situation. The results can then be used to aid in the design of the multi-module endoscope hardware, but also in tuning the controllers.

8.3 Scalability

A big improvement to the module would be downscaling the dimensions in the radial direction to be better suitable for MIS and NOTES applications. Downscaling will give problems with the size of the chambers, which determine the bending force, and the space required for guiding instruments. Although a thinner module might be able to achieve more bending with less bending force due to decreased bending stiffness, lower forces also mean that external influences will become bigger. The weight of the module will have more impact as well. Solutions to these problems have to be found in order for the endoscope to be used in clinical practice.

Downscaling is also required for the airlocks, which were placed ouside of the endoscope. The stiff connector pieces in between the individual modules are a good place for encorporating the airlocks. The airlocks therefore have to be made smaller, which makes fabrication more difficult. This means that it is not guaranteed that the smaller airlocks work as expected and that more tests are required. Next to the airlocks, the integration of pneumatic logic would benefit the downscaling of the endoscope significantly, as explained in chapter 7. Pneumatic logic has not been treated in this project and is therefore a subject for further research.

8.4 Other recommendations

The steerable robotic endoscope is designed for use with path planning, that can be used to avoid obstacles and make sure that the target is reached correctly. Path planning has only been mentioned and was not treated in this project. Combing path planning with the soft robotic endoscope will greatly improve the usability and safety of the device, but also poses some difficulties that require more research. At the time of writing, the path planning problem is being researched by other students.

The stiffening capabilities of MOLLUSC were dropped, but a variable stiffening mechanism would be beneficial for the control of the endoscope when force or precision is required. The small study that was added in appendix A already showed some preliminary findings in literature. Layer jamming on the outside of the endoscope seems the most promising method. More research in the direction of stiffening for the soft robotic endoscope is recommended, especially in the direction of layer jamming.

Other improvements to the endoscope might be changes to the sequential addressing algorithm to improve the speed of the endoscope, the addition of more pressure regulators to pressurize chambers in parallel (if possible within the limited volume), and improving the UI to be more user-friendly.

9 Conclusion

A first proof of concept of a scalable, MR-compatible, soft robotic endoscope for MIS and NOTES applications was realized and validated. Although not all set requirements were met, insight was gained in the actuation principles of the snake-like pneumatic actuators that form the basic endoscopic modules. It was found that the pneumatic (MR-compatible) 3-chamber inner sheath modules were most suitable for endoscopic applications when controllability and scalability were taken into account.

The endoscopic modules that were realized proved to be repeatable in behaviour and a physical model of the modules could therefore be used reliably. Steering the bending angle of the endoscopic modules based on the physical model was possible within a maximum error of 4°, or 13% of the maximum bending at 1 bar of input pressure. This error was mostly due to the slight differences in the fabrication of the modules. Greater accuracy can be achieved when the model of each module is adjusted based on characterization.

Validation of the multi-module endoscope showed that the module design and the influence of external factors did not permit the use of the whole expected actuation range. Nevertheless, the endoscope could be steered towards targets within a decreased range if manual compensation, or feedback, is used. Several options are available to improve the steerability of the soft robotic endoscope, such as the increase of allowable chamber pressure, the decrease of the influence of factors as the pneumatic tubing and weight of the modules, and the optimization of the module design within its outer dimensions.

Downscaling of the endoscope for application in clinical practice can most likely be enhanced with novel integrated airlocks and pneumatic logic that aid in decreasing the pneumatic tubing size and number of pneumatic tubes. It was demonstrated that steering the endoscope with airlocks is possible in principle and that the amount of required hardware can be decreased significantly compared to the classical control setup. Integrating the airlocks in the endoscope itself requires further research, because the fabrication requires high precision and the integrated airlocks are prone to leaks. The use of pneumatically activated airlocks ensures that the endoscope is MR-compatible.

The insights gained in this study can be used to improve the steerability of the endoscopic modules and scale the soft robotic endoscope in order to make it suitable for MR assisted MIS and NOTES.

A A literature study on stiffening for the soft robotic endoscope

There exist endoscopes that support stiffness adjustability. The STIFF-FLOP and MOLLUSC designs use coffee powder in a latex membrane and applied vacuum to change the stiffness of the modules. In this way, the endoscope can remain flexible, but can stiffen when force or precision is required. MOLLUSC can control the stiffness of the modules in several levels. The Neoguide design (Peters et al., 2018), while not soft, uses a passive and an active mode. In the active mode the endoscope is relatively stiff and can be controlled, in the passive mode the endoscope is less stiff. Independent stiffness control of each segment is not reported (Gifari, 2018). Outside of endoscopic applications, stiffening in soft robotics is a large topic of research and many studies have been performed on the different stiffening methods (Manti et al., 2016). This is why a small literature study was performed to determine the best stiffening method for the soft robotic endoscope. This eventually formed the starting point for the work of other students.

A.1 Available stiffening methods

In order to ensure the right stiffness for when force or precision is required, the endoscope should support a stiffening method. In soft robotics, many types of stiffening are known. Manti et al. (Manti et al., 2016) categorise several actuation methods, some of which can be used for stiffening. A distinction is made between two types of stiffening methods: active-passive and semiactive.

Active-passive based stiffening works by combining actuation with a passive structure that prevents deformation. By actuation, the total structure stiffens. Antagonistic actuation can be used as well.

Semiactive stiffening works by modulating the mechanical properties of the material itself.

Manti et al. (Manti et al., 2016) describe the following actuation (active-passive) and stiffening (semiactive) categories:

- Flexible fluidic actuators
- Shape memory material
- Electroactive polymers
- Tendon-driven actuators
- Material jamming
- Electro- and magnetorheological materials
- Low melting point materials

Of these categories, flexible fluidic actuators, tendon-driven actuators, and material jamming are the only methods suitable for the MR-compatible soft robotic endoscope. The other methods require electric or magnetic activation, or require phase changes which take time. While the activation time is not necessarily a problem, the surgical application of the endoscope will benefit significantly from a faster stiffening method.

The endoscopic module that is used is a type of flexible fluidic actuator and its stiffness is therefore expected to increase when it is actuated. This stiffening is not controllable independent

of the bending angle however and an extra, independent, stiffening method is required. The same is true for the tendon-driven actuators. This means that material jamming, because it works independent of module actuation, is the most suitable method of achieving different levels of stiffness in the actuator of the soft robotic endoscope.

Gifari (Gifari, 2018) achieved multilevel stiffening by using granular jamming with jamming sacs placed within the pneumatic chambers of the actuator modules. These jamming sacs consisted of a latex membrane filled with coffee powder and can be seen in figure A.1. By applying a vacuum, the granules lock together and provide stiffness for the larger structure. Cianchetti et al. (Cianchetti et al., 2014) achieved independent stiffening with similar jamming sacs within the central cylinder, leaving no space for surgical instruments. Both studies show that independent stiffening is achievable, but results show that there are still problems with repeatability in actuation due to the added stiffening methods.

Figure A.1: The granular jamming sac used for stiffening the MOLLUSC design (Gifari, 2018)

Another material jamming method is layer jamming. Instead of using small granules that interlock, layer jamming uses the friction between layers of materials such as paper. The principle of actuation remains similar to granular jamming. By applying a vacuum, the layers are locked together and provide stiffness. Examples of the application of layer jamming are shown by Santiago et al. (Santiago et al., 2016), Sadati et al. (Sadati et al., 2015), and Kim et al. (Kim et al., 2012).

A.2 The stiffening method for the soft robotic endoscope

The layer jamming mechanism seems the most promising of the stiffening methods, especially when looking at the results of Kim et al. (Kim et al., 2012) which can be applied outside of the endoscope. This layer jamming design can be seen in figure A.2. Keeping the stiffening mechanism outside of the endoscope would mean that it will not interfere with the space required for routing pressure tubes. It also means that the mechanism is sufficiently isolated from the exact endoscopic module design that it can be designed independently. More research should therefore be performed in the direction of layer jamming on the surface of the soft robotic endoscope.

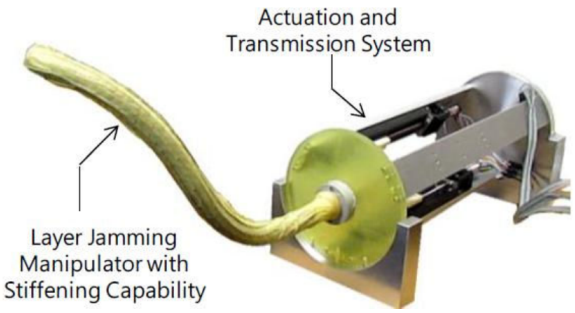

Figure A.2: The snake-like manipulator including layer jamming as designed by Kim et al. (Kim et al., 2012)

B The physical model of the soft robotic endoscopic module

The bending direction and angle of the endoscopic modules can be calculated using the geometry of the module, the material parameters, and the applied pressures P_1, P_2, and P_3. The following model is an extended version of the static model of Fraś et al. (Fraś et al., 2014):

Geometry parameters and material properties

$D_m = 0.025$ Module diameters [m]

$D_{Chm} = 0.005$ Chamber diameter [m]

$D_{Ccm} = 0.008$ Central cylinder diameter [m]

$L_{Chm} = 0.030$ Length of a pneumatic chamber [m]

$I = 16.87705e-9$ Second moment of area [m^4]

$E = 82737.1$ Young's modulus of Ecoflex 00-50 [Pa]

$r = 0.00825$ Radius to the center of a pneumatic chamber [m]

$C_1 = [-r;0]$ Direction of the force vector of chamber 1 [m]

$C_2 = [\cos(60)r; -\cos(30)r]$ Direction of the force vector of chamber 2 [m]

$C_3 = [\cos(60)r; \cos(30)r]$ Direction of the force vector of chamber 3 [m]

$A_{ch} = (\frac{D_{Chm}}{2})^2\pi$ Crossectional area of a chamber [m^2]

$A_m = (\frac{D_m}{2})^2\pi - 3A_{ch} - (\frac{D_{Ccm}}{2})^2\pi$ Area of the silicone part of the module's cross section [m^2]

Forces, moments and the changes in geometry

$F_1 = 100000P_1A_{ch}$ Force of chamber 1 [N]

$F_2 = 100000P_2A_{ch}$ Force of chamber 2 [N]

$F_3 = 100000P_3A_{ch}$ Force of chamber 3 [N]

$M = C_1F_1 + C_2F_2 + C_3F_3$ The moment vector [Nm]

$M_{abs} = \sqrt{(M(1)^2 + M(2)^2)}$ The moment [Nm]

$\Delta l = \frac{F_1+F_2+F_3}{A_mE}L_{Chm}$ The extra length of a module due to elongation [m]

$I_{factor} = (\frac{L_{Chm}}{L_{Chm}+\Delta l})^3$ The compensation for the change in second moment of area

$I = II_{factor}$ The compensated second moment of area [m^4]

The constant curvature approximation

$\kappa = \frac{M_{abs}}{EI}$ The curvature of the module [$\frac{1}{m}$]

$\rho = \frac{1}{\kappa}$ The radius of curvature of the module [m]

$\theta = \frac{L_{Chm}+\Delta l}{\rho}$ The bending angle of the module [rad]

$\phi = \arctan(\frac{M(2)}{M(1)})$ The bending direction of the module [rad]

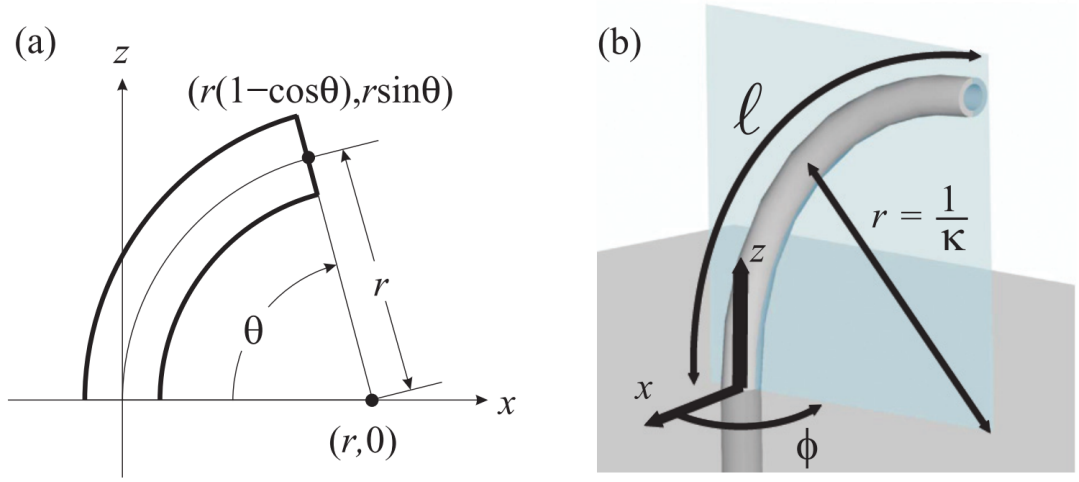

Figure B.1: The constant curvature approximation showing how three parameters are required to fully define the shape of a bending soft robotic snake-like module. (a) is a side view showing how the bending angle θ and the curvature radius can be used to find the location of the tip of the module. (b) is a 3D view showing that the radius is directly related to the curvature κ of the module and that the bending direction is defined by ϕ. While the bending direction ϕ is independent of the other variables, κ, l and θ are all linked. Only two of these three variables are necessary for completely defining the bending shape. In constant curvature kinematics κ, l and ϕ are used. r and θ can be calculated when desired. (Webster III and Jones, 2010)

C The connector piece design with integrated airlocks

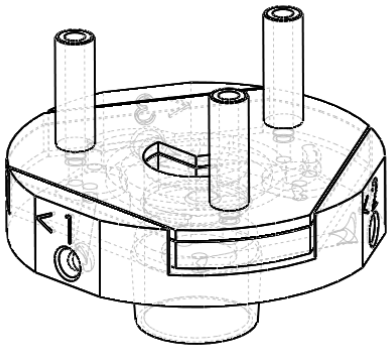

(a) The connector piece with integrated airlocks

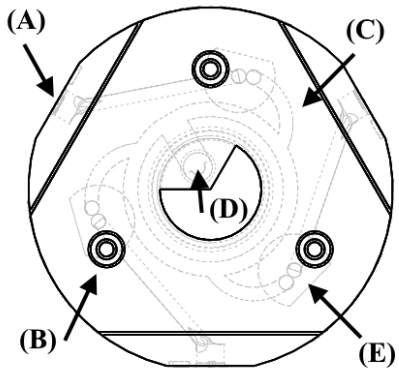

(b) (A) is the input for the control pressure, (B) is the pressure output to the chamber, (C) is the internal air channel that distributes the supply, (D) is the input for the supply pressure, and (E) is the miniature airlock mechanism.

Figure C.1: Assembly view

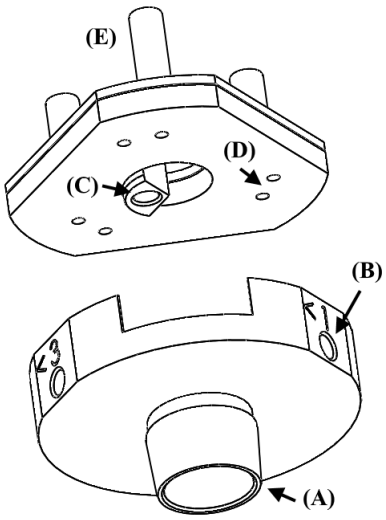

(a) (A) is the empty central cylinder, (B) is the input for the control pressure, (C) is the input for the supply pressure, (D) are the supply input and output of a single airlock, and (E) is the output to the chamber.

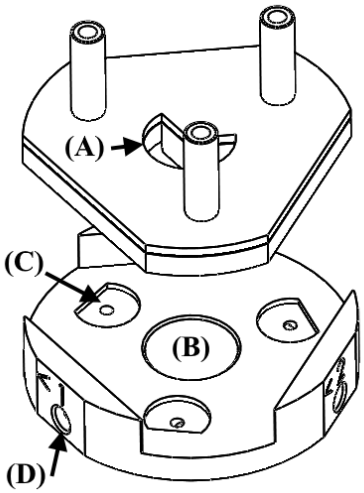

(b) (A) is the empty central cylinder in the top part, (B) is the empty central cylinder in the bottom part, (C) is the control pressure reservoir of a single airlock, and (D) is the input for the control pressure.

Figure C.2: Exploded view

Bibliography

Abidi, H., G. Gerboni, M. Brancadoro, J. Fraś, A. Diodato, M. Cianchetti, H. Wurdemann, K. Althoefer and A. Menciassi (2018), Highly dexterous 2-module soft robot for intra-organ navigation in minimally invasive surgery, in *International Journal of Medical Robotics and Computer Assisted Surgery*, volume 14, pp. 1–9.

Allaix, Y. M. M. E., M. A. Bonino, S. Arolfo, M. Morino and A. Arezzo (2017), Total Mesorectal Excision Using the STIFF-FLOP Soft and Flexible Robotic Arm in Cadaver Models, in *Surgical Endoscopy*, volume 31, pp. 339–356.

Bernth, J. E., A. Arezzo and H. Liu (2017), A Novel Robotic Meshworm with Segment-Bending Anchoring for Colonoscopy, in *IEEE Robot. Autom. Lett.*, volume 2, pp. 1–1.

Blinman, T. (2010), Incisions do not simply sum, in *Surgical Endoscopy*, volume 24, Springer, pp. 1746–1751.

Boškoski, I. and G. Costamagna (2018), Endoscopy robotics: current and future applications, in *Digestive Endoscopy*, pp. 0–1.

Brown, E., N. Rodenberg, J. Amend, A. Mozeika, E. Steltz, M. R. Zakin, H. Lipson and H. M. Jaeger (2010), Universal robotic gripper based on the jamming of granular material, in *Proceedings of the National Academy of Sciences*, volume 107, pp. 18809–18814.

Cianchetti, M., T. Ranzani, G. Gerboni, C. Falco, I. D. Laschi, S. Member and A. Menciassi (2013), STIFF-FLOP Surgical Manipulator: mechanical design and experimental characterization of the single module, in *IEEE/RSJ International Conference on Intelligent Robots and Systems (IROS)*, pp. 3576–3581.

Cianchetti, M., T. Ranzani, G. Gerboni, T. Nanayakkara, K. Althoefer, P. Dasgupta and A. Menciassi (2014), Soft Robotics Technologies to Address Shortcomings in Today's Minimally Invasive Surgery: The STIFF-FLOP Approach, in *Soft Robotics*, volume 1, pp. 122–131.

De Falco, I., M. Cianchetti and A. Menciassi (2017), A soft multi-module manipulator with variable stiffness for minimally invasive surgery, in *Bioinspiration and Biomimetics*, volume 12.

Elsayed, Y., A. Vincensi, C. Lekakou, T. Geng, C. M. Saaj, T. Ranzani, M. Cianchetti and A. Menciassi (2014), Finite Element Analysis and Design Optimization of a Pneumatically Actuating Silicone Module for Robotic Surgery Applications, in *Soft Robotics*, volume 1, pp. 255–262.

Fraś, J., J. Czarnowski, M. Maciaś and J. Główka (2014), Static modeling of multisection soft continuum manipulator for stiff-flop project, in *Advances in Intelligent Systems and Computing*, volume 267, pp. 365–375.

Fraś, J., J. Czarnowski, M. Maciaś, J. Główka, M. Cianchetti and A. Menciassi (2015), New STIFF-FLOP module construction idea for improved actuation and sensing, in *Proceedings - IEEE International Conference on Robotics and Automation*, pp. 2901–2906.

Gerboni, G., T. Ranzani, A. Diodato, G. Ciuti, M. Cianchetti and A. Menciassi (2015), Modular soft mechatronic manipulator for minimally invasive surgery (MIS): overall architecture and development of a fully integrated soft module, in *Meccanica*, volume 50, pp. 2865–2878.

Gifari, M. W. (2018), Study on the Design of Soft Surgical Robots for Endoscopic NOTES Applications, University of Twente.

Henning, A. K. (2007), Concepts for micropneumatic and microhydraulic logic gates, in *Proceedings of SPIE, Microfluidics, BioMEMS, and Medical Microsystems V*, volume 6465, SPIE.

Holdar, M. and E. D. Engeberg (2018), Sot Robotics: Fiber Reinforced Soft Pneumatic Multidirectional Manipulators, Designing, Fabricating, and Testing.

Jansen, J. (2018), Endoscopic end effector control using soft actuator, University of Twente.

Johnson, P. J., C. M. Rivera Serrano, M. Castro, R. Kuenzler, H. Choset, S. Tully and U. Duvuri (2013), Demonstration of Transoral Surgery in Cadaveric Specimens with the Medrobotics Flex System, in *The Laryngoscope*, volume 123, The American Layngological, Rhinological and Otological Society, Inc., pp. 1168–1172.

Jones, B. A. and I. D. Walker (2006), Kinematics for Multisection Continuum Robots, in *IEEE Trans. on Robot.*, volume 22, pp. 43–55.

Kim, Y., S. S. Cheng, M. Diakite, R. P. Gullapalli, J. M. Simard and J. P. Desai (2017), Toward the Development of a Flexible Mesoscale MRI-Compatible Neurosurgical Continuum Robot, in *IEEE Trans. Robot.*, volume 33, pp. 1386–1397.

Kim, Y. J., S. Cheng, S. Kim and K. Iagnemma (2012), Design of a Tubular Snake-like Manipulator with Stiffening Capability by Layer Jamming, in *IEEE/RSJ International Conference on Intelligent Robots and Systems*, pp. 4251–4256.

Laparoscope (2019), Laparoscope.
http://www.dishafertility.com/laparoscopy.html

Laschi, C., J. Rossiter, F. Iida, M. Cianchetti and L. Margheri (2016), Soft Robotics: Trends Applications and Challenges, in *Proceedings of the Soft Robotics Week*.

Loeve, A., P. Breedveld and J. Dankelman (2010), Scopes too flexible and too stiff, in *IEEE Pulse*, volume 1, pp. 26–41.

Manti, M., V. Cacucciolo and M. Cianchetti (2016), Stiffening in Soft Robotics - A Review of the State of the Art, in *IEEE Robot. & Autom. Magazine*, volume 23, pp. 93–106.

Naghibi, H., M. W. Gifari, W. Hoitzing, J. W. Lageveen, D. van As, S. Stramigioli and M. Abayazid (2019), Development of a multilevel stiffness soft robotics module with force haptic feedback for endoscopic applications, in *Proceedings of the IEEE international conference on robotics and automation (ICRA)*.

NDI, N. D. I. (2019), Aurora electromagnetic tracking system.
http://www.ndigital.com/medical/wp-content/uploads/sites/4/2013/12/Aurora.pdf

Peters, B. S., P. R. Armijo, C. Krause, S. A. Choudhury and D. Oleynikov (2018), Review of emerging surgical robotic technology, in *Surgical endoscopy*, Springer, pp. 1–20.

PIAP (2019), The 'STIFF-FLOP' Project.
https://piap.pl/en/badanie/the-stiff-flop-project/

Polygerinos, P., Z. Wang, K. C. Galloway, R. J. Wood and C. J. Walsh (2015), Soft robotic glove for combined assistance and at-home rehabilitation, in *Robotics and Autonomous Systems*, volume 73, Elsevier, pp. 135–143.

RaM (2019a), MRI-compatible robotics.
https://www.ram.ewi.utwente.nl/research/project/mri-compatible-robotics.html

RaM (2019b), MURAB.
https://www.ram.ewi.utwente.nl/research/project/murab.html

Robertson, M. A. and J. Paik (2017), New soft robots really suck: vacuum powered systems empower diverse capabilities, in *Science Robotics*, volume 2, eaan6357.

Rösch, T., A. Adler, H. Pohl, E. Wettschureck, M. Koch, B. Wiedenmann and N. Hoepffner (2008), A motor-driven single-use colonoscope controlled with a hand-held device: a feasibility study in volunteers, in *Gastrointestinal Endoscopy*, volume 67, Elsevier, pp. 1139–1146.

Rus, D. and M. T. Tolley (2015), Design, fabrication and control of soft robots, in *Nature*, volume 521, pp. 467–475.

Sadati, S. M. H., S. E. Naghibi, A. Shiva, Y. Noh, A. Gupta, I. D. Walker, K. Althoefer and T. Nanayakkara (2017), A geometry deformation model for braided continuum manipulators, in *Frontiers in Robotics and AI*, volume 4, p. 22.

Sadati, S. M. H., Y. Noh, S. E. Naghibi, K. Althoefer and T. Nanayakkara (2015), Stiffness Control of Soft Robotic Manipulator for Minimally Invasive Surgery (MIS) Using Scale Jamming, in *International Conference on Intelligent Robotics and Applications*, Springer, pp. 141–151.

Santiago, J. L. C., I. S. Godage and I. D. Walker (2016), Soft Robots and Kangaroo Tails: Modulating Compliance in Continuum Structures via Mechanical Layer Jamming, in *Soft Robotics*, volume 3, pp. 54–63.

Seah, T. E. T., T. N. Do, N. Takeshita, K. Y. Ho and S. J. Phee (2018), Flexible Robotic Endoscopy Systems and the Future Ahead, in *arXiv preprint arXiv:1703.05569*, pp. 521–536.

Suzumori, K., S. Iikura and H. Tanaka (1991), Flexible microactuator for miniature robots, in *Proceedings. IEEE Micro Electro Mechanical Systems*, pp. 204–209.

Trivedi, D., C. D. Rahn, W. M. Kier and I. D. Walker (2008), Soft robotics: Biological inspiration, state of the art, and future research, in *Applied Bionics and Biomechanics*, volume 5, pp. 99–117.

Webster III, R. J. and B. A. Jones (2010), Design and Kinematic Modeling of Constant Curvature Continuum Robots: A Review, in *The International Journal of Robotics Research*, volume 29, pp. 1661–1683.

Whitmer, L. M. (2007), Clinical Anatomy of the Large Intestine, in *Centers for Osteopathic Research & Education*.

Woodward, S. (2017), Cancel PWM DAC ripple with analog subtraction. https://www.edn.com/design/analog/4459116/Cancel-PWM-DAC-ripple-with-analog-subtraction